

The Euclidean Adler Function and its Interplay with $\Delta\alpha_{\text{QED}}^{\text{had}}$ and α_s

M. Davier,^a D. Díaz-Calderón,^b B. Malaescu,^c A. Pich,^b A. Rodríguez-Sánchez,^{c,d,e,f}
Z. Zhang^a

^a *Université Paris-Saclay, CNRS/IN2P3, IJCLab, 91405 Orsay, France*

^b *Departament de Física Teòrica, IFIC, Universitat de València – CSIC
Parque Científico, Catedrático José Beltrán 2, E-46980 Paterna, Spain*

^c *LPNHE, Sorbonne Université, Université Paris Cité, CNRS/IN2P3, Paris, France*

^d *Sorbonne Université, CNRS, Laboratoire de Physique Théorique et Hautes Energies (LPTHE),
F-75252 Paris, France*

^e *SISSA International School for Advanced Studies, Via Bonomea 265, 34136, Trieste, Italy*

^f *INFN, Sezione di Trieste, SISSA, Via Bonomea 265, 34136, Trieste, Italy*

ABSTRACT: Three different approaches to precisely describe the Adler function in the Euclidean regime at around 2 GeVs are available: dispersion relations based on the hadronic production data in e^+e^- annihilation, lattice simulations and perturbative QCD (pQCD). We make a comprehensive study of the perturbative approach, supplemented with the leading power corrections in the operator product expansion. All known contributions are included, with a careful assessment of uncertainties. The pQCD predictions are compared with the Adler functions extracted from $\Delta\alpha_{\text{QED}}^{\text{had}}(Q^2)$, using both the DHMZ compilation of e^+e^- data and published lattice results. Taking as input the FLAG value of α_s , the pQCD Adler function turns out to be in good agreement with the lattice data, while the dispersive results lie systematically below them. Finally, we explore the sensitivity to α_s of the direct comparison between the data-driven, lattice and QCD Euclidean Adler functions. The precision with which the renormalisation group equation can be tested is also evaluated.

Contents

1	Introduction	2
2	Theoretical framework	4
3	The perturbative Adler function	6
3.1	Light-quark contributions	7
3.1.1	Leading massless contributions	7
3.1.2	Strange mass corrections	9
3.1.3	Heavy-quark mass corrections	10
3.2	Heavy-quark contributions	14
3.3	QED corrections	17
3.4	Compilation	18
4	Adler function based on the experimental ratio $R(s)$ and lattice data	18
4.1	Experimental ratio $R(s)$	20
4.2	Lattice Adler function	21
5	Comparison of the three different approaches to $D(Q^2)$	23
6	Nonperturbative corrections to the perturbative Adler function	24
6.1	Light-quark correlators	25
6.2	Charm correlator	27
6.3	Discussion	27
7	Determination of α_s from the Adler function	28
7.1	Averages	30
7.2	Theoretical uncertainties	33
7.3	Results	33
8	Conclusions	36
A	Compilation of perturbative coefficients	38
A.1	Running of α_s , quark masses and decoupling relations	38
A.2	Light-quark loop coefficients	39
A.3	Heavy-quark loop coefficients	40
B	Interplay of $\bar{\Pi}^{08}$ with perturbative QCD	42
C	Fit results for α_s using lattice data	43

1 Introduction

Two-point functions are among the most basic objects that one can define within a Quantum Field Theory (QFT). Every possible action encodes associated distributions for them. From the phenomenological point of view, a particularly interesting one is the two-point correlation function of two vector neutral quark currents,

$$\Pi_{ij}^{\mu\nu}(q) \equiv i \int d^4x e^{-iqx} \langle 0 | T (\bar{q}_i(x) \gamma^\mu q_i(x) \bar{q}_j(0) \gamma^\nu q_j(0)) | 0 \rangle = (q^\mu q^\nu - g^{\mu\nu} q^2) \Pi_{ij}(s \equiv q^2). \quad (1.1)$$

Even in the partonic approximation, this is in the absence of quantum corrections and neglecting quark masses, these two-point correlation functions are divergent and depend on an arbitrary subtraction prescription. This approximation makes sense as the leading term of an Operator Product Expansion (OPE) [1–3] which is well defined for large Euclidean momenta, $Q^2 = -q^2$ and leads to¹

$$\Pi_{ij}^{\text{part}}(Q^2) = -\frac{N_C}{12\pi^2} \delta_{ij} [\log(Q^2) + C_{\text{subtraction}}], \quad (1.2)$$

where N_C is the number of quark colours. In order to avoid unphysical subtraction ambiguities, it is convenient to define the object of study in this work, the Euclidean Adler function [4]:

$$D_{ij}(Q^2) \equiv -12\pi^2 Q^2 \frac{d\Pi_{ij}(Q^2)}{dQ^2}, \quad (1.3)$$

which gives in the partonic limit

$$D_{ij}^{\text{part}}(Q^2) = N_C \delta_{ij}. \quad (1.4)$$

The most important corrections in the Standard Model (SM) come from strong interactions. At large Euclidean momenta, far enough from the non-analytic behaviour in the distributions induced by hadrons, deviations from asymptotic freedom are described by perturbative QCD (pQCD), so that the leading corrections are simply given by $\delta D_{ij}(Q^2) = N_C \delta_{ij} \frac{\alpha_s(Q^2)}{\pi}$. For light quarks $i, j \leq 3$, $D_{ij}^L(Q^2)$, the perturbative QCD description breaks down in the infrared region: the low-energy hadron dynamics is not well described by approximately-free quarks and gluons. Our knowledge about it at very low energies (there are no physical singularities at $Q^2 = 0$) implies that $D_{ij}(Q^2 \rightarrow 0) = 0$.²

¹In the rest of the complex plane $\Pi_{ij}(Q^2)$ can be obtained by analytic continuation. We take $\text{Arg}(Q^2) \in [-\pi, \pi)$ and $q^2 = e^{i\pi} Q^2$, so that $\text{Arg}(q^2) \in [0, 2\pi)$. In this way, $\text{Im}\Pi(|Q^2|e^{-i\pi}) = \frac{1}{2i}[\Pi(|Q^2|e^{-i\pi}) - \Pi(|Q^2|e^{i\pi})]$.

²Let us note that if one defines $\alpha_s^{\text{eff}}(Q^2) \equiv \pi \left(\frac{D_{ii}(Q^2)}{N_C} - 1 \right)$, then $\alpha_s^{\text{eff}}(0) = -\pi$, which per-se does not tell us any new fundamental knowledge about strong interactions.

Low-energy Effective Field Theories (EFTs), such as Chiral Perturbation Theory [5–7], give some nontrivial information about the infrared behaviour of $D_{ij}^L(Q^2)$, but their predictive power is limited, especially at intermediate energies. For massive quarks, $i, j > 3$, $D_{ij}^H(Q^2)$, a perturbative QCD description is known to give a precise description of the Adler function even in the neighbourhood of $Q^2 \rightarrow 0$ [8–11], since quark masses regularize, at least up to a certain extent, the gluon singularities associated to infrared propagators.

Other powerful nonperturbative methods can also be used to obtain $D_{ij}(Q^2)$. Numerical simulations in a discretized space-time lattice [12] allow for a precise computation of the two-point functions at Euclidean momenta without relying on perturbation theory. Indeed huge efforts are recently being made to compute the electromagnetic correlator,

$$\Pi(Q^2) \equiv \sum_{i,j} Q_i Q_j \Pi_{ij}(Q^2), \quad (1.5)$$

where Q_i is the electromagnetic charge of the associated quark in units of e (e.g. $Q_1 = \frac{2}{3}$), since it plays a fundamental role in our understanding of the anomalous magnetic moment of the muon and in the so-called hadronic running of the QED coupling [13–23]. Currently the predictive power of lattice methods becomes severely limited as one goes above $Q \sim 2 - 3$ GeVs due to discretization effects, leading to an interesting complementarity with respect to pQCD.

Similar motivations have increased the knowledge of $\Pi(Q^2)$ obtained from another powerful nonperturbative method, the dispersive data-driven approach, which mainly uses electron-positron data to determine $\Pi(Q^2)$ [24–29]. A well-known limitation in the current precision comes from a series of tensions involving electron-positron data. Besides the long-established discrepancy between $e^+e^- \rightarrow \pi^+\pi^-$ and $\tau^- \rightarrow \pi^-\pi^0\nu_\tau$ data (invoking an isospin rotation) [30], there are significant tensions among different e^+e^- data sets (mainly KLOE vs BABAR, for the same 2π channel). Additionally, there is a clear discrepancy between the experimental value of $(g-2)_\mu$ and the theoretical SM prediction obtained when using e^+e^- data to evaluate the Hadronic Vacuum Polarization (HVP) contribution (even after inflating uncertainties to account for the KLOE-BABAR tension). Finally, further tensions arise between e^+e^- data and lattice evaluations of both the hadronic running of the QED coupling and again the HVP contribution to $(g-2)_\mu$ [13, 14, 31–34].

In this work we study analytically the Euclidean Adler function, in the Q^2 region where perturbation theory is expected to be valid, with the aim of comparing it to both the dispersive Adler function $D(Q^2)$ obtained with the DHMZ compilation of data [28] and the one obtained from recently published lattice results for the hadronic running of the QED coupling [14].

On the one hand, assuming the validity of pQCD at a certain Euclidean momentum Q , one can check whether the description is consistent with the other approaches. On the other hand, assuming that the other approaches are correct, we have a uniquely clean window to learn about the onset of the asymptotic regime and the value of the associated QCD coupling. We start by introducing the overall theoretical framework to connect the different descriptions of the Euclidean Adler functions and the HVP. This is done in Sec. 2. In Sec. 3 we perform a comprehensive study of the perturbative Adler function in the

regime we are interested in, combining many existing results. Then, in Sec. 4, we explain in detail how the data-driven and the lattice Adler functions are obtained, and in Sec. 5 we compare them with the perturbative expression. Power corrections are discussed in Sec. 6. Finally an exploration to the sensitivity of the comparison to the strong coupling and discussion about some possible fitting strategies can be found in Sec. 7. Conclusions and final remarks are presented in Sec. 8.

2 Theoretical framework

Let us start by connecting the needed descriptions and observables related to the HVP. The hadronic running of the QED coupling can be defined in terms of the electromagnetic correlator $\Pi(Q^2)$ as follows,

$$\Delta\alpha_{\text{had}}(Q^2) \equiv 4\pi\alpha \bar{\Pi}(Q^2), \quad \bar{\Pi}(Q^2) = \Pi(0) - \Pi(Q^2), \quad (2.1)$$

with $\alpha = \alpha(0) = 1/137.035999084(21)$ [35]. Since both the hadronic running of $\alpha(Q^2)$ and the Adler function are defined in terms of the electromagnetic correlator (*cf.* Eq. (1.3)), it is straightforward to relate both of them,

$$D(Q^2) \equiv \sum_{i,j} Q_i Q_j D_{ij}(Q^2) = 3\pi Q^2 \frac{d\Delta\alpha_{\text{had}}(Q^2)}{\alpha dQ^2}. \quad (2.2)$$

Alternatively,

$$\Delta\alpha_{\text{had}}(Q^2) - \Delta\alpha_{\text{had}}(Q_0^2) = \frac{\alpha}{3\pi} \int_{Q_0^2}^{Q^2} \frac{dQ'^2}{Q'^2} D(Q'^2). \quad (2.3)$$

On the other hand, it can be shown that the ratio of hadronic and muonic production cross sections in e^+e^- annihilation is directly related to the imaginary part of $\Pi(Q^2)$. Formally, it is defined as

$$R(s) \equiv \frac{3s}{4\pi\alpha} \sigma^0(e^+e^- \rightarrow \text{hadrons} (+\gamma)) = 12\pi \text{Im}\Pi(Q^2 = s e^{-i\pi}), \quad (2.4)$$

where $\sigma^0(e^+e^- \rightarrow \text{hadrons} (+\gamma))$ refers to the so-called “bare” hadronic cross section in electron-positron annihilation, subtracting the vacuum polarization contribution to the photon propagator and the Initial State Radiation (and ISR-FSR interference) but including all Final State Radiation.

Thus, in order to relate $R(s)$ with $D(Q^2)$ and $\Delta\alpha_{\text{had}}(Q^2)$, we have to relate the imaginary part of the analytic continuation of $\Pi(Q^2)$ with $\Pi(Q^2)$ itself. This is accomplished by using dispersion relations, which combine our knowledge of the analytic structure of the electromagnetic correlator, $\Pi(Q^2)$, with its known asymptotic behaviour. Indeed, the partonic picture, see Eq. (1.2), is valid at very high energies and $\Pi(Q^2)$ is an analytic function in the whole complex plane except for a branch cut starting at the hadronic threshold,³

³If QED effects are included, the threshold becomes $Q_{\text{th}}^2 = -m_\pi^2$, corresponding to the $\pi^0\gamma$ channel.

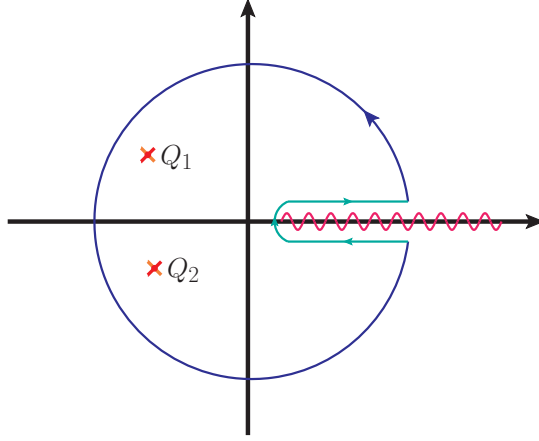


Figure 1. Circuit of integration of $\frac{1}{2\pi i} W(Q^2; Q_1^2, Q_2^2) \cdot \Pi_{ij}(Q^2)$ in the $q^2 = -Q^2$ complex plane.

$Q_{\text{th}}^2 = -4m_\pi^2$. As a consequence, we can integrate $\Pi(Q^2)$ in the complex plane along any contour as long as we avoid this cut. We may also weight the integral with some function

$$W(Q^2; Q_1^2, Q_2^2) = \frac{1}{(Q^2 - Q_1^2)(Q^2 - Q_2^2)}, \quad (2.5)$$

which is analytic in the complex plane except for the two poles. Then, integrating along the contour in Fig. 1 and using the Residue Theorem, we get

$$\frac{1}{2\pi i} \int_{\mathcal{C}} dQ^2 \frac{\Pi_{ij}(Q^2)}{(Q^2 - Q_1^2)(Q^2 - Q_2^2)} = \frac{\Pi_{ij}(Q_2^2)}{Q_2^2 - Q_1^2} + \frac{\Pi_{ij}(Q_1^2)}{Q_1^2 - Q_2^2}. \quad (2.6)$$

We may separate the different contributions to the contour integral as

$$\begin{aligned} & \frac{1}{2\pi i} \oint_{|Q^2|=Q_0^2} dQ^2 \frac{\Pi_{ij}(Q^2)}{(Q^2 - Q_1^2)(Q^2 - Q_2^2)} + \frac{1}{2\pi i} \left(\int_{|Q_{\text{th}}^2|e^{-i\pi}}^{|Q_0^2|e^{-i\pi}} - \int_{|Q_{\text{th}}^2|e^{i\pi}}^{|Q_0^2|e^{i\pi}} \right) dQ^2 \frac{\Pi_{ij}(Q^2)}{(Q^2 - Q_1^2)(Q^2 - Q_2^2)} \\ &= \frac{\Pi_{ij}(Q_2^2)}{Q_2^2 - Q_1^2} + \frac{\Pi_{ij}(Q_1^2)}{Q_1^2 - Q_2^2}. \end{aligned} \quad (2.7)$$

For $|Q_0^2| \rightarrow \infty$ one can easily show that the first term in the first line goes to zero by using the partonic description. Performing a change of variables and using the Schwarz reflection principle in the second term, one arrives at

$$\frac{1}{\pi} \int_{|Q_{\text{th}}^2|}^{\infty} dQ'^2 \frac{\text{Im}\Pi_{ij}(Q'^2 e^{-i\pi})}{(Q^2 + Q_1^2)(Q^2 + Q_2^2)} = -\frac{\Pi_{ij}(Q_2^2) - \Pi_{ij}(Q_1^2)}{Q_2^2 - Q_1^2}. \quad (2.8)$$

Starting from this expression, one can obtain dispersion relations for different objects by choosing different values of Q_1^2 and Q_2^2 . Choosing either Q_1^2 or Q_2^2 to be 0 leads to a dispersion relation for the correlator $\Pi(Q^2)$,

$$\frac{\Pi(Q^2) - \Pi(0)}{Q^2} = -\frac{1}{\pi} \int_{|Q_{\text{th}}^2|^2}^{\infty} dQ'^2 \frac{\text{Im}\Pi(Q'^2 e^{-i\pi})}{Q'^2(Q'^2 + Q^2)}. \quad (2.9)$$

A dispersion relation for the Adler function can be obtained by differentiating $\Pi(Q^2)$ (cf. Eq. (1.3)) in Eq. (2.9) or by choosing $Q_1^2 = Q_2^2 + \delta$ with $\delta \rightarrow 0$ in the weight function. Either way, one obtains⁴

$$D_{ij}(Q^2) = 12\pi Q^2 \int_{|Q_{th}^2|}^{\infty} dQ'^2 \frac{\text{Im}\Pi_{ij}(Q'^2 e^{-i\pi})}{(Q'^2 + Q^2)^2}. \quad (2.10)$$

It is then straightforward to write an equation for the data-driven determination of the Euclidean Adler function using Eq. (2.10) and Eq. (2.4),

$$D(Q^2) = Q^2 \int_{s_{th}}^{\infty} ds \frac{R(s)}{(s + Q^2)^2}. \quad (2.11)$$

Finally, $\Delta\alpha_{\text{had}}(Q^2)$ is also related to $R(s)$ through the dispersion relation of Eq. (2.9) and Eq. (2.4),

$$\Delta\alpha_{\text{had}}(Q^2) = \frac{\alpha Q^2}{3\pi} \int_{s_{th}}^{\infty} ds \frac{R(s)}{s(s + Q^2)}. \quad (2.12)$$

3 The perturbative Adler function

The perturbative Adler function has been the subject of many studies in different energy regimes, since it is directly linked to different precisely known inclusive observables [36]. At order α_s^2 and beyond, the coefficients in the expansion depend on the renormalization scheme. For practical purposes, the $\overline{\text{MS}}$ scheme is usually adopted due to its computational simplicity. In the limit of n_f massless quarks and no massive ones, the corresponding Adler functions are known up to (and including) five loops (*i.e.* order α_s^4).

The real world contains six quark flavours with a striking hierarchy of quark masses:

$$m_{u,d} \ll m_s \ll \Lambda_{\text{QCD}} \ll m_c \ll m_b \ll m_t, \quad (3.1)$$

where Λ_{QCD} is the QCD scale, so that perturbative QCD does not make sense below it. In mass-independent renormalization schemes such as the $\overline{\text{MS}}$, the perturbative series with six quark flavours does not give a very accurate approximation to the QCD Adler function at $|Q^2| \ll m_t^2$. This is a consequence of the lack of decoupling associated with this type of schemes, which leads to $\log(m_t^2/Q^2)$ factors that slow down and eventually break the perturbative series (*e.g.* see [37] for a pedagogical introduction to the problem). If one wants to keep track of the full quark-mass dependence of the Adler function [38], useful for example for the perturbative running of $\Delta\alpha^{\text{had}}(Q^2)$ from $Q \sim 2.5 \text{ GeV}$ to $Q = M_Z$ [39], one possibility is employing a renormalization scheme that automatically performs the decoupling of heavy masses, such as MOM, at the cost of more complex calculations and less known perturbative corrections. Alternatively, one can still work in the $\overline{\text{MS}}$ scheme by introducing a series of QCD effective field theories with different number n_f of massless quark flavours, which need to be matched at the corresponding quark-mass thresholds. The

⁴Let us note that the result holds for complex momenta, which promotes the analytic continuation of the Adler function to an observable.

decoupling of heavy masses is then implemented by hand and the massless Adler function can be supplemented with the corresponding power-suppressed corrections from the heavy quark masses. The small contributions from the non-zero light-quark masses can be taken into account through perturbative expansions in powers of m_q^2/Q^2 .

Since the other methods analyzed in this work are also more powerful below $|Q^2| \sim 5 \text{ GeV}^2$, we will focus on the Adler function $D(Q^2)$ at $|Q^2| < 4m_c^2$. In the next subsections we study the different perturbative Adler functions $D_{ij}(Q^2)$ separately, first focusing on those with $i, j < 4$ (light-quark contributions) and then on the heavy ones, $i, j > 3$ (heavy-quark contributions). Eventually we add the leading QED corrections, put them together and also explain why the mixed ($i < 4, j > 3$ and vice-versa) contributions to $D(Q^2)$ are very suppressed.

3.1 Light-quark contributions

3.1.1 Leading massless contributions

For light flavours $i, j < 4$, the $\overline{\text{MS}}$ scheme with $n_f = 3$ massless quarks gives an accurate description of the perturbative Adler function in the energy range $\Lambda_{\text{QCD}}^2 \ll Q^2 \ll 4m_c^2$. The flavour-diagonal ($i = j$) correlators contribute to $D(Q^2)$ through the so-called non-singlet topology with the two electromagnetic currents connected by one quark loop. The result can be written as

$$D_{ii}^{L,(0)}(Q^2) = N_C \left\{ 1 + \sum_{n=1} \sum_{p=0}^{n-1} K_{n,p} \left(\frac{\alpha_s(\mu^2)}{\pi} \right)^n \log^p(Q^2/\mu^2) \right\}, \quad (3.2)$$

with μ the renormalization scale. Additional disconnected diagrams with each current in a separate quark loop (singlet topology), which are also present for $i \neq j$, start to contribute at order α_s^3 , but with three massless quarks the flavour trace of both quark loops cancels in the sum ($Q_u + Q_d + Q_s = 0$), leading to a completely negligible effect of $\mathcal{O}\left(\alpha_s^3 \frac{m_s^4}{Q^4}\right)$ for $D(Q^2)$ once the non-zero masses are taken into account.

The (0) superscript indicates that we have not yet incorporated any quark mass correction. Since the Adler function is independent of the renormalization scale, one can trivially reconstruct the coefficients $K_{n,p}$ with $p > 0$ from those with $p = 0$, simply taking into account the Renormalization Group Equation (RGE) satisfied by the strong coupling:

$$\mu \frac{d\alpha_s}{d\mu} = \alpha_s \beta(\alpha_s), \quad \beta(\alpha_s) = \sum_{n=1} \beta_n \left(\frac{\alpha_s}{\pi} \right)^n. \quad (3.3)$$

The coefficients of the Adler function are known up to five loops, *i.e.* at $\mathcal{O}(\alpha_s^4)$, while the QCD β function has been already computed to $\mathcal{O}(\alpha_s^5)$. We collect the values of $K_{n \leq 4, 0}$, $\beta_{n \leq 5}$ and the rest of perturbative coefficients in App. A. Since we need to truncate the series, a residual scale dependence (of the first unaccounted order) remains. In order to avoid higher-order corrections enhanced by large logarithms of the renormalization scale, one should set $\mu^2 = \xi^2 Q^2$ with ξ^2 a number of order 1. The exact choice is however ambiguous and a priori arbitrary, just as it is the exact scheme choice of how to minimally

subtract when renormalizing. Modifying the residual scale dependence through the variation of ξ^2 in a reasonable interval around unity can then be used to estimate perturbative uncertainties [40]. One has

$$D_{ii}^{L,(0)}(Q^2) = N_C \left(1 + \sum_{n=1} K_n(\xi^2) \left(\frac{\alpha_s(\xi^2 Q^2)}{\pi} \right)^n \right), \quad (3.4)$$

with

$$K_n(\xi^2) = \sum_{p=0}^{n-1} K_{n,p} \log^p(1/\xi^2). \quad (3.5)$$

In order to numerically evaluate the Adler functions below the charm threshold, we then need $\alpha_s(\mu^2)$ with $n_f = 3$. The standard input is however $\alpha_s(M_Z^2)$ with $n_f = 5$. One can translate one into another by supplementing the RGE given above with the decoupling relations,

$$\alpha_s^{(n_f-1)}(\mu^2) = \alpha_s^{(n_f)}(\mu^2) \left\{ 1 + \sum_{k=1}^k \sum_{n=0}^k d_{kn} \left[a_s^{(n_f)}(\mu^2) \right]^k \log^n(\mu^2/M_q^2) \right\}, \quad (3.6)$$

$$m_q^{(n_f-1)}(\mu^2) = m_q^{(n_f)}(\mu^2) \left\{ 1 + \sum_{k=2}^k \sum_{n=0}^k h_{kn} \left[a_s^{(n_f)}(\mu^2) \right]^k \log^n(\mu^2/M_q^2) \right\}, \quad (3.7)$$

where $M_q \equiv m_q^{(n_f)}(\mu^2)$ is the running mass of the heavy quark that has been integrated out and $a_s^{(n_f)} \equiv \alpha_s^{(n_f)}/\pi$, which is also needed as input. The running masses satisfy the following renormalization group equation

$$\mu \frac{dm_q}{d\mu} = -m_q \gamma(\alpha_s), \quad \gamma(\alpha_s) = \sum_{n=1} \gamma_n \left(\frac{\alpha_s}{\pi} \right)^n, \quad (3.8)$$

where the perturbative γ_n coefficients are known up to $n = 5$. We will take as extra input $m_c(m_c^2) = 1.275(5)$ GeV and $m_b(m_b^2) = 4.171(20)$ GeV from the FLAG lattice review [41–54] and perform the decoupling at $\mu = m_q(m_q^2)$. Quark-mass uncertainties are small enough to be negligible. Our results for $\alpha_s(Q^2) \equiv \alpha_s^{(n_f=3)}(Q^2)$ and $D_{ii}^{L,(0)}(Q^2)$ are given in Table 1 for several choices of $\alpha_s^{(n_f=5)}(M_Z^2)$ and Q , at different orders in the strong coupling. We have checked that the $\alpha_s(Q^2)$ values fully agree with the corresponding values obtained with RUNDEC [55]. In Fig. 2 we show the corresponding Q^2 dependence for $\alpha_s^{(n_f=5)}(M_Z^2) = 0.115, 0.120$, at $\mathcal{O}(\alpha_s^5)$, adding as perturbative uncertainties the quadratic sum of variations due to changing K_5 in a conservative interval $(-125, 675)$ and $\xi^2 \in (0.5, 2)$ [36]. The range chosen for K_5 includes the values advocated by renormalon models, Padé approximants, effective charges and conformal mappings [56–62], but also allows for a correction of opposite sign. The interval of variation for the renormalization scale is conventional for low-energy analyses, e.g. see [63, 64]. This is partially justified by the fact that taking a too small value for ξ^2 , one would be using an ill-defined expansion parameter $\alpha_s(\xi^2 Q^2)$ without any real justification, leading to unreasonable uncertainties.⁵ Alternative

⁵In this sense the observed blow-up in the uncertainty at $Q^2 \approx 1 \text{ GeV}^2$ when α_s is increased, it is a consequence of the variation of ξ^2 towards too small values.

prescriptions to circumvent this issue, such as asymmetric scale variations, can be found in the literature. See for example Ref. [65].

			$D_{ii}^{L,(0)}(Q^2)$					
$\alpha_s^{(n_f=5)}(M_Z^2)$	Q	$\alpha_s(Q^2)$	0	1	2	3	4	5
0.115	1.0	0.4227	3	3.4036	3.4927	3.5392	3.5874	3.6238
	1.5	0.3197	3	3.3053	3.3562	3.3764	3.3921	3.4011
	2.0	0.2751	3	3.2627	3.3005	3.3133	3.3219	3.3262
0.120	1.0	0.5277	3	3.5039	3.6427	3.7332	3.8504	3.9606
	1.5	0.3681	3	3.3515	3.4191	3.4498	3.4776	3.4958
	2.0	0.3085	3	3.2946	3.3420	3.3601	3.3738	3.3813

Table 1. Values of $\alpha_s(Q^2)$ with $n_f = 3$ (left) at different scales Q (in GeV units) for two input choices of $\alpha_s^{(n_f=5)}(M_Z^2)$. The corresponding values of $D_{ii}^{L,(0)}(Q^2)$ are given in the right columns at different orders in $\alpha_s(Q^2)$. Our central value for the fifth-order coefficient, $K_5 = 275$, has been adopted in the last column.

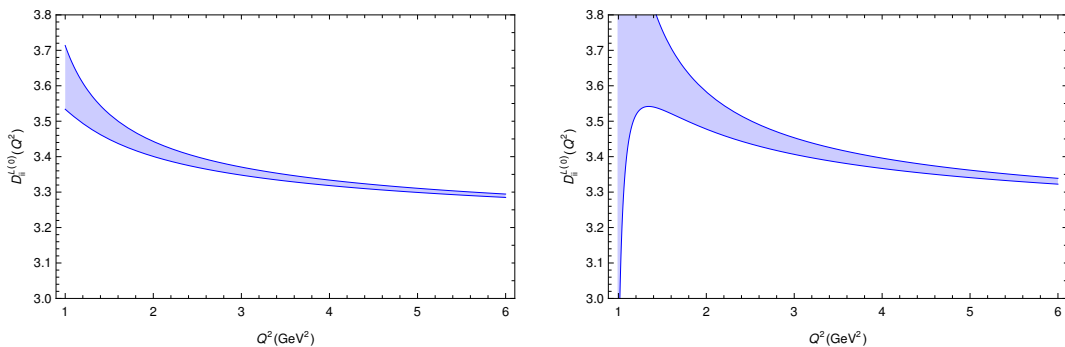


Figure 2. Q^2 (GeV² units) dependence of $D_{ii}^{L,(0)}(Q^2)$ in perturbative $n_f = 3$ massless QCD, at $\mathcal{O}(\alpha_s^5)$, for $\alpha_s^{(n_f=5)}(M_Z^2) = 0.115$ (left) and 0.120 (right), including perturbative uncertainties.

3.1.2 Strange mass corrections

The light quark masses are not exactly zero, and this leaves a small imprint, fully dominated by the strange quark mass. Let us then safely neglect the tiny effects suppressed by $\mathcal{O}(\frac{m_{u,d}^2}{Q^2})$. Taking $\mu^2 = Q^2$ one has [36]

$$\Delta_{m_s} D_{33}^L(Q^2) = -3N_C \frac{m_s^2(Q^2)}{Q^2} \sum_n (2c_n^{L+T} + e_n^{L+T} + f_n^{L+T}) \left(\frac{\alpha_s(Q^2)}{\pi} \right)^n + \mathcal{O}\left(\frac{m_s^4}{Q^4}\right), \quad (3.9)$$

where $m_s(Q^2) \equiv m_s^{(n_f=3)}(Q^2)$ and the coefficients are once again shown in App. A. Numerical values for the associated corrections at different Q , taking as input $m_s(\mu_0^2) = (92.03 \pm 0.88)$ MeV at $\mu_0 = 2$ GeV [41, 42, 46, 47, 49, 66–70], can be found in Table 2.⁶

⁶Once again, we have cross-checked that both the strong coupling values and the strange quark mass ones fully agree with the corresponding ones obtained by using instead the RUNDEC package [55].

Let us note the very bad behaviour of the perturbative series (3.9), which appears to show its asymptotic behaviour from the first terms. Fortunately, the whole mass correction is very suppressed by the small value of the strange quark mass and its electric charge. We will take as central value the average between truncating at $\mathcal{O}(\alpha_s^2)$ and $\mathcal{O}(\alpha_s^3)$ and half their difference as an additional perturbative uncertainty. The associated Q^2 dependence, together with our estimated error bars are shown in Fig. 3.

				$\Delta_{m_s} D_{33}^L(Q^2)$			
$\alpha_s^{(n_f=5)}(M_Z^2)$	Q	$\alpha_s(Q^2)$	$m_s(Q^2)$	0	1	2	3
0.115	1.0	0.4227	0.1177	-0.2495	-0.4062	-0.6007	-0.8821
	1.5	0.3197	0.09997	-0.07994	-0.1179	-0.1536	-0.1926
	2.0	0.2751	0.09203	-0.03811	-0.0537	-0.0663	-0.0781
0.120	1.0	0.5277	0.1276	-0.2932	-0.5229	-0.8790	-1.5223
	1.5	0.3681	0.1018	-0.08289	-0.1282	-0.1772	-0.2390
	2.0	0.3085	0.09203	-0.03811	-0.0556	-0.0714	-0.0881

Table 2. Values of $\alpha_s(Q^2)$ and $m_s(Q^2)$ with $n_f = 3$ (left) for several choices of Q (GeV units) and $\alpha_s^{(n_f=5)}(M_Z^2)$. The corresponding values of $\Delta_{m_s} D_{33}^L(Q^2)$ are shown in the right columns at different perturbative orders.

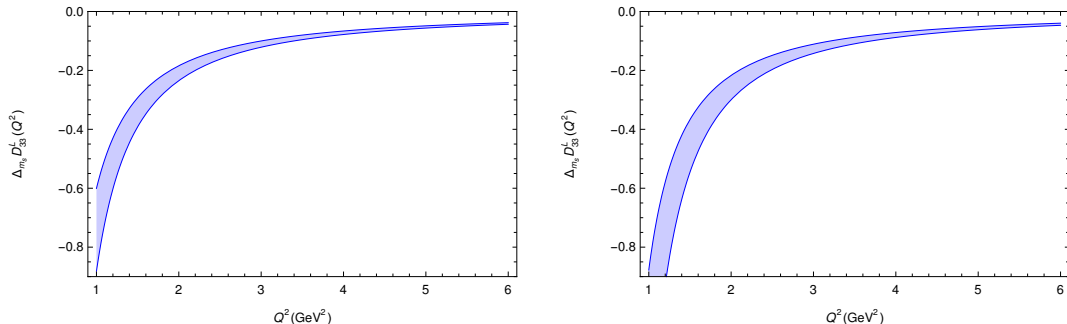


Figure 3. Q^2 dependence of $\Delta_{m_s} D_{33}^L(Q^2)$ for $\alpha_s^{(n_f=5)}(M_Z^2) = 0.115$ (left) and 0.120 (right).

3.1.3 Heavy-quark mass corrections

Internal heavy-quark loops induce charm-mass corrections into the light-quark correlators, which are suppressed by powers of $\frac{Q^2}{4m_c^2}$ and start to contribute at $\mathcal{O}(\alpha_s^2)$. In order to take into account these small, but sizable when approaching the charm threshold, contributions to the Euclidean Adler function, we can use the known results at order α_s^2 for the associated contributions to $R(s)$. Two distinct topologies appear there. One corresponds to the four-quark cut, ρ_R , which starts at $s = 4m_c^2$. The second corresponds to the vertex correction ρ_V , which, in the chiral limit, starts at $s = 0$. The exact expressions can be found in [71]. Taking into account that these are the only cuts induced by those topologies, one can

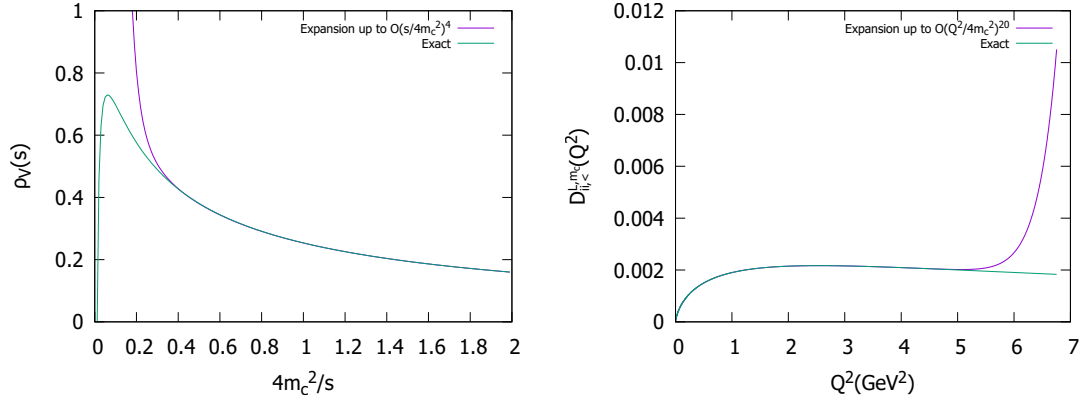


Figure 4. *Left:* Comparison between the exact form of $\rho_V(s)$ and its expansion in the limit $4m_c^2/s \rightarrow \infty$. As can be checked, they are equal for $4m_c^2/s > 1$. *Right:* Comparison between $D_{ii,<}^{L,m_c}(Q^2)$ computed numerically and computed analytically, using the expansion (3.11) for $\rho_V(s)$, and performing an expansion in $Q^2/4m_c^2$ afterwards. The input value $\alpha_s^{(n_f=5)}(M_Z^2) = 0.1184$ has been adopted.

reconstruct the associated contribution to the Adler function by using the same kind of dispersion relation as above:

$$\begin{aligned}
D_{ii,<}^{L,m_c}(Q^2) &= Q^2 \int_{s_{th}}^{\infty} ds \frac{\delta R_q(s)}{(s+Q^2)^2} \\
&= N_C C_F T_F Q^2 \left(\int_0^{4m_c^2} ds \frac{\rho_V(s)}{(s+Q^2)^2} + \int_{4m_c^2}^{\infty} ds \frac{\rho_R(s) + \rho_V(s)}{(s+Q^2)^2} \right) \left(\frac{\alpha_s(\mu^2)}{\pi} \right)^2,
\end{aligned} \tag{3.10}$$

where $C_F T_F = 2/3$. As expected, for small enough values of Q^2 both integrals admit expansions in powers of $\frac{Q^2}{4m_c^2}$. For the former, the $Q^2 \ll 4m_c^2$ expansion can only be performed after integration, since $s \in (0, 4m_c^2)$. However, one can first expand $\rho_V(s)$ in powers of $\frac{s}{4m_c^2}$ whose leading, next-to-leading and next-to-next-to-leading terms can also be found in Refs. [72, 73]:

$$\begin{aligned}
\rho_V(s) &= \frac{1}{45} \left[\frac{22}{5} + \log\left(\frac{m_c^2}{s}\right) \right] \frac{s}{m_c^2} - \frac{1}{1680} \left[\frac{1303}{420} + \log\left(\frac{m_c^2}{s}\right) \right] \left(\frac{s}{m_c^2}\right)^2 \\
&+ \frac{1}{28350} \left[\frac{1643}{630} + \log\left(\frac{m_c^2}{s}\right) \right] \left(\frac{s}{m_c^2}\right)^3 - \frac{1}{332640} \left[\frac{32429}{13860} + \log\left(\frac{m_c^2}{s}\right) \right] \left(\frac{s}{m_c^2}\right)^4 \\
&+ \mathcal{O}\left(\frac{s}{m_c^2}\right)^5.
\end{aligned} \tag{3.11}$$

In the left panel of Fig. 4 we show how truncating at this order is already an excellent approximation in the needed interval. Using that expanded version, it is straightforward to analytically integrate in s and then expand in powers of $\frac{Q^2}{4m_c^2}$. One finds

$$\begin{aligned}
D_{ii,<}^{L,m_c}(Q^2) = & N_C C_F T_F \left(\frac{\alpha_s(\mu^2)}{\pi} \right)^2 \left\{ \left[-\frac{923574439}{2161120500} + \frac{4}{45} \zeta_2 + \frac{124666}{155925} \log(2) - \frac{8}{45} \log^2(2) \right. \right. \\
& + \frac{8}{45} \log^2 \left(\frac{m_c}{Q} \right) + \frac{136}{225} \log \left(\frac{m_c}{Q} \right) \left. \right] \frac{Q^2}{4m_c^2} + \left[\frac{1211942621}{2161120500} + \frac{2}{105} \zeta_2 - \frac{250907}{1091475} \log(2) \right. \\
& - \frac{4}{105} \log^2(2) + \frac{1093}{11025} \log \left(\frac{m_c}{Q} \right) + \frac{4}{105} \log^2 \left(\frac{m_c}{Q} \right) \left. \right] \left(\frac{Q^2}{4m_c^2} \right)^2 + \left[-\frac{1023355847}{2161120500} \right. \\
& + \frac{32}{4725} \zeta_2 + \frac{4084286}{16372125} \log(2) - \frac{64}{4725} \log^2(2) + \frac{45856}{1488375} \log \left(\frac{m_c}{Q} \right) \\
& \left. + \frac{64}{4725} \log^2 \left(\frac{m_c}{Q} \right) \right] \left(\frac{Q^2}{4m_c^2} \right)^3 + \dots \left. \right\} + \mathcal{O} \left(\frac{Q^2}{4m_c^2} \alpha_s^3 \right). \tag{3.12}
\end{aligned}$$

In the right panel of Fig. 4, the agreement between this expansion and the result obtained computing the integral numerically, using the full expression for $\rho_V(s)$, can be seen. Following an analogous criteria as for the light quarks, we will estimate uncertainties from higher orders by changing μ between $\frac{m_c(m_c^2)}{\sqrt{2}}$ and $\sqrt{2} m_c(m_c^2)$.⁷

Similar arguments can be used for the second term. In this case, the expansion in powers of Q^2 can be performed before or after integration. In the first case, the integrals can be computed numerically using the full expressions for $\rho_V(s)$ and $\rho_R(s)$. On the other hand, to perform the Q^2 expansion after integration, we have expanded $\rho^V(s) + \rho^R(s)$ first at large s ,

$$\begin{aligned}
\rho_R(s) + \rho_V(s) = & \left[-\frac{1}{4} \log \left(\frac{m_c^2}{s} \right) + \zeta_3 - \frac{11}{8} \right] + \left(\frac{m_c^2}{s} \right)^2 \left[-\frac{3}{2} \log \left(\frac{m_c^2}{s} \right) - 6\zeta_3 + \frac{13}{2} \right] \\
& + \left(\frac{m_c^2}{s} \right)^3 \left[-\frac{4}{9} \log^2 \left(\frac{m_c^2}{s} \right) + \frac{28}{27} \log \left(\frac{m_c^2}{s} \right) + \frac{8}{9} \zeta(2) + \frac{68}{81} \right] + \mathcal{O} \left(\frac{m_c^2}{s} \right)^4, \tag{3.13}
\end{aligned}$$

which agrees with Ref. [71], in order to integrate them analytically. Both ways yield very similar results since, as can be seen in Fig. 5, the expansion of $\rho_V(s) + \rho_R(s)$ agrees very well with the full expression. The contribution to the Adler function then is:

$$\begin{aligned}
D_{ii,>}^{L,m_c}(Q^2) = & N_C C_F T_F \left\{ \left[-\frac{40523}{41472} + \frac{1}{288} \zeta_2 + \frac{7}{8} \zeta_3 + \frac{955}{1728} \log(2) - \frac{1}{144} \log^2(2) \right] \frac{Q^2}{4m_c^2} \right. \\
& + \left[\frac{2673461}{2592000} - \frac{1}{180} \zeta_2 - \frac{13}{16} \zeta_3 - \frac{12497}{21600} \log(2) + \frac{1}{90} \log^2(2) \right] \left(\frac{Q^2}{4m_c^2} \right)^2 \\
& + \left[-\frac{66851}{64800} + \frac{1}{144} \zeta_2 + \frac{31}{40} \zeta_3 + \frac{1283}{2160} \log(2) - \frac{1}{72} \log^2(2) \right] \left(\frac{Q^2}{4m_c^2} \right)^3 \\
& \left. + \dots \right\} \left(\frac{\alpha_s(\mu^2)}{\pi} \right)^2 + \mathcal{O} \left(\frac{Q^2}{4m_c^2} \alpha_s^3 \right). \tag{3.14}
\end{aligned}$$

⁷This is just one possible choice to circumvent the overestimated uncertainty due to an ill-defined expansion parameter that one would have if $\mu = \frac{m_c(m_c^2)}{2}$ were taken. For heavy quarks an alternative way of achieving this, based on using different scale choices for $m_c(\mu^2)$ and $\alpha_s(\mu^2)$, which is useful to avoid underestimating uncertainties in fits with combined moments, can be found in Refs. [74, 75].

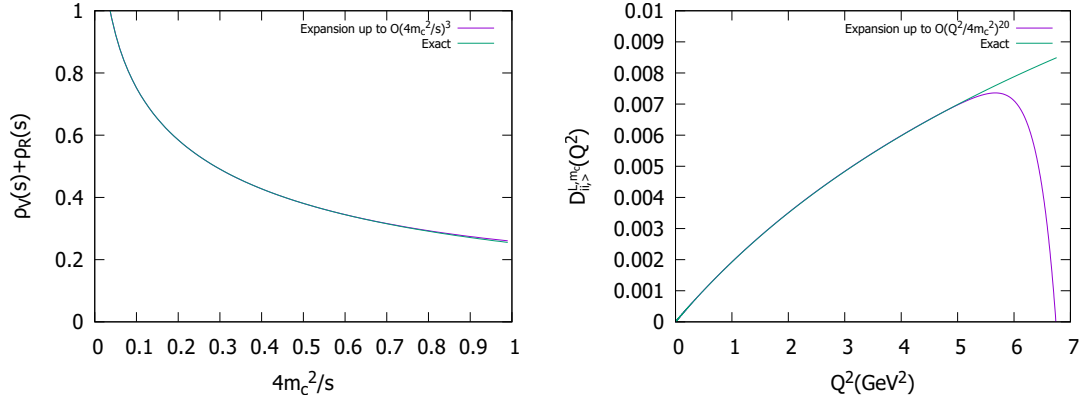


Figure 5. *Left:* Comparison between the exact form of $\rho_V(s) + \rho_R(s)$ and its expansion in the limit $4m_c^2/s \rightarrow 0$. As can be seen, they are equal for $0 < 4m_c^2/s < 1$. *Right:* Comparison between $D_{ii}^{L,m_c}(Q^2)$ computed numerically and computed analytically, using the expansion (3.13) for $\rho_V(s) + \rho_R(s)$ and performing an expansion in $Q^2/4m_c^2$ afterwards. The input value $\alpha_s^{(n_f=5)}(M_Z^2) = 0.1184$ has been adopted.

The comparison between this expansion and the exact result is plotted on Fig. 5. As expected, the expansion in powers of $Q^2/4m_c^2$ diverges from the exact result near threshold.

It is worth making a parenthesis to note how this second integral fully dominates if one takes instead $Q^2 \gg 4m_c^2$. In that case one may use the expansion (3.13) of $\rho_R(s) + \rho_V(s)$ at $s \gg m_c^2$. The leading term diverges as $s \rightarrow \infty$, generating a large α_s^2 contribution to $D(Q^2)$ that grows logarithmically at large Q^2 :

$$N_C C_F T_F Q^2 \int_{4m_c^2}^{\infty} ds \frac{-\frac{1}{4} \log \frac{m_c^2}{s} + \zeta_3 - \frac{11}{8}}{(s + Q^2)^2} \approx N_C C_F T_F \left(-\frac{1}{4} \log \frac{m_c^2}{Q^2} + \zeta_3 - \frac{11}{8} \right). \quad (3.15)$$

However one should keep in mind that the strong coupling with $n_f = 3$ flavors should not be used as expansion parameter far above the charm threshold. In this limit, at order α_s^2 , one then has

$$\begin{aligned} D_{ii}^L(Q^2) &= D_{ii}^{L,(n_f=3)}(\alpha_s^{(n_f=3)}(\mu^2), Q^2) + D_{ii}^{L,m_c}(Q^2) \\ &= N_C \left[1 + \frac{\alpha_s^{(n_f=3)}(\mu^2)}{\pi} + \left(\frac{\alpha_s^{(n_f=3)}(\mu^2)}{\pi} \right)^2 \left(K_{2,0}^{(n_f=3)} - \frac{\beta_1^{(n_f=3)}}{2} \log \frac{\mu^2}{Q^2} \right) \right. \\ &\quad \left. + \left(\frac{\alpha_s^{(n_f=3)}(\mu^2)}{\pi} \right)^2 C_F T_F \left(-\frac{1}{4} \log \frac{m_c^2}{Q^2} + \zeta_3 - \frac{11}{8} \right) + \mathcal{O}(\alpha_s^3) \right] \\ &= N_C \left[1 + \frac{\alpha_s^{(n_f=4)}(\mu^2)}{\pi} + \left(\frac{\alpha_s^{(n_f=4)}(\mu^2)}{\pi} \right)^2 \left(K_{2,0}^{(n_f=4)} - \frac{\beta_1^{(n_f=4)}}{2} \log \frac{\mu^2}{Q^2} \right) \right] + \mathcal{O}(\alpha_s^3) \\ &= D_{ii}^{L,(n_f=4)}(\alpha_s^{(n_f=4)}(\mu^2), Q^2) + \mathcal{O}(\alpha_s^3), \end{aligned} \quad (3.16)$$

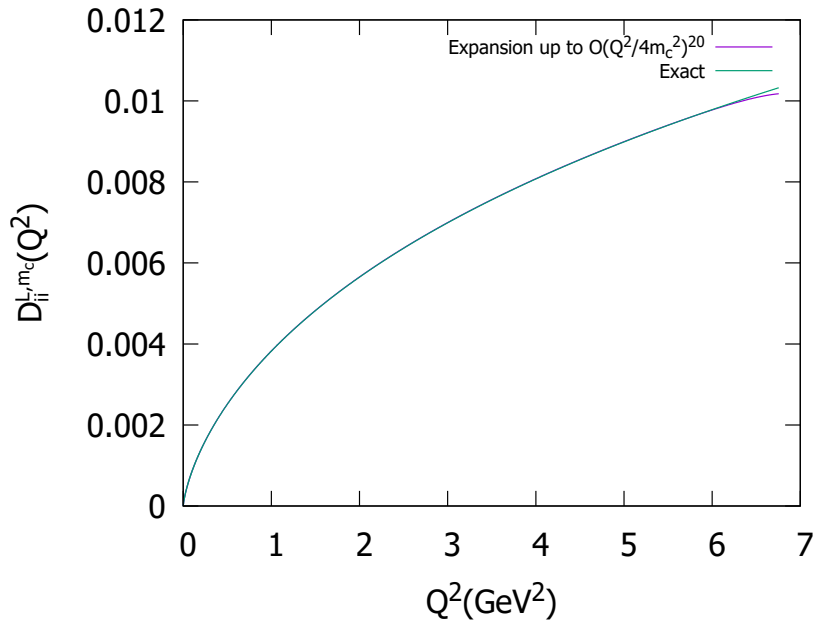


Figure 6. Comparison between $D_{ii}^{L,m_c}(Q^2) = D_{ii,<}^{L,m_c}(Q^2) + D_{ii,>}^{L,m_c}(Q^2)$ computed numerically and computed analytically, using the expansions and performing an expansion in $Q^2/4m_c^2$ afterwards. The input value $\alpha_s^{(n_f=5)}(M_Z^2) = 0.1184$ has been adopted.

which shows how the logarithm of the charm mass is properly reabsorbed into the $n_f = 4$ strong coupling, through the QCD matching conditions, while the constant α_s^2 term reproduces the known n_f dependence of $K_{2,0}$.

The total heavy-quark contribution to the light Adler function, $D_{ii}^{L,m_c}(Q^2) = D_{ii,<}^{L,m_c}(Q^2) + D_{ii,>}^{L,m_c}(Q^2)$, is plotted in Fig. 6. The expanded expression in powers of $Q^2/(4m_c^2)$ turns out to provide an excellent approximation to the exact numerical result in the full range of Q^2 values analysed.

3.2 Heavy-quark contributions

In this section we benefit from the many works devoted to computing the needed coefficients for the Adler function induced by heavy quarks [8, 76–87]. One may write the low-energy expansion of the heavy-quark loops as

$$\Pi_{ii} = \frac{3}{16\pi^2} \sum_j \bar{C}_j(\mu) z^j(\mu), \quad (3.17)$$

where

$$\bar{C}_j(\mu) = \sum_n \bar{C}_j^{(n)}(\mu) \left(\frac{\alpha_s(\mu^2)}{\pi} \right)^n, \quad (3.18)$$

and

$$z(\mu) = -\frac{Q^2}{4m_i^2(\mu^2)}. \quad (3.19)$$

The associated Adler function is then

$$D_{ii}(Q^2) = -\frac{9}{4} \sum_j (-1)^j j \bar{C}_j(\mu) \left(\frac{Q^2}{4m_i^2(\mu^2)} \right)^j. \quad (3.20)$$

The $\bar{C}_j^{(0,1,2)}$ coefficients are known up to $j = 30$ [79, 80] and $\bar{C}_j^{(3)}$ up to $j = 3$ [81–84]. The contribution to $\bar{C}_4^{(3)}$ from topologies associated to quark-connected (non-singlet) contributions has also been computed [85], and very good approximations to the coefficients $\bar{C}_j^{(3)}$ from $j = 5$ to $j = 10$ are also known [86, 87]. They are typically given at the renormalization scale $\mu = m_c(m_c^2)$, but one can then trivially recover them at arbitrary scales by using RGEs. We compile them in App. A. In Fig. 7 we show the associated Adler function up to different orders in α_s , cutting the series at $j = 10$.⁸ The series is observed to stabilize after including the two-loop corrections. We also show in Fig. 8 the convergence of the energy expansion at three loops, truncating at several values of j . As expected, the energy series breaks down slightly below $Q^2 \sim 4m_c^2$. We find that one actually needs to keep quite high orders. Nevertheless, for practical purposes $j = 10$ is high enough to safely neglect higher orders below $Q^2 \sim 5.5 \text{ GeV}^2$. In order to estimate perturbative uncertainties we will vary the renormalization scale in the interval $\mu = (\frac{1}{\sqrt{2}}, 1) m_c(m_c^2)$.⁹ This, together with the uncertainty coming from the input value $m_c(m_c^2) = 1.275(5) \text{ GeV}$, are the main sources of error from this contribution.

Finally, from $j = 4$ a singlet topology with a massless (three-gluon) cut also appears at four loops, whose leading contribution at $Q^2 \ll m_c^2$ is driven by a known logarithm [88]

$$\Pi_{cc}^s(Q^2) = -\frac{17d_{abc}d_{abc}}{243000} \left(\frac{Q^2}{4m_c^2} \right)^4 \left(\log \frac{Q^2}{m_c^2} + C \right) \left(\frac{\alpha_s(\mu^2)}{\pi} \right)^3, \quad (3.21)$$

with $d_{abc}d_{abc} = 40/3$. While this leads to a logarithmic divergence in the associated coefficient, the limit $Q \rightarrow 0$ does not give any problems for the Adler function itself. One finds

$$D_{cc}^s(Q^2) \approx \frac{17\pi^2 d_{abc}d_{abc}}{20250} \left(\frac{Q^2}{4m_c^2} \right)^4 \left(4 \log \frac{Q^2}{m_c^2} + 1 + 4C \right) \left(\frac{\alpha_s(\mu^2)}{\pi} \right)^3. \quad (3.22)$$

Based on the known relative values of the constant coefficients in the analogous axial-current singlet contributions (starting at α_s^2) [79], one expects $C = 0 \pm 3$, so the predictive power for this tiny correction is very limited. Taking into account this uncertainty and the one from changing the residual scale dependence of $\mathcal{O}(\alpha_s^4)$ in the interval $\mu = \sqrt{2}(\frac{1}{2}, 1) m_c(m_c^2)$, one finds the result shown in Fig 9.

Adding everything up, one finds the contribution to the Adler function associated with the charm mass. The suppressed (both by $\frac{Q^2}{4m_b^2}$ and the electromagnetic charge factor Q_b^2)

⁸For the fourth loop and $j > 4$ we take the approximate coefficients obtained in [87], which succeeded in giving an excellent prediction for the nowadays exactly known $j = 4$ [85].

⁹The rationale behind this asymmetric choice is that $j = 10$ is not precise enough near $Q^2 \sim 5.5 \text{ GeV}^2$ if $\mu = \sqrt{2} m_c(m_c^2)$ is taken, which has nothing to do with the perturbative uncertainties of the Taylor coefficients that we want to estimate.

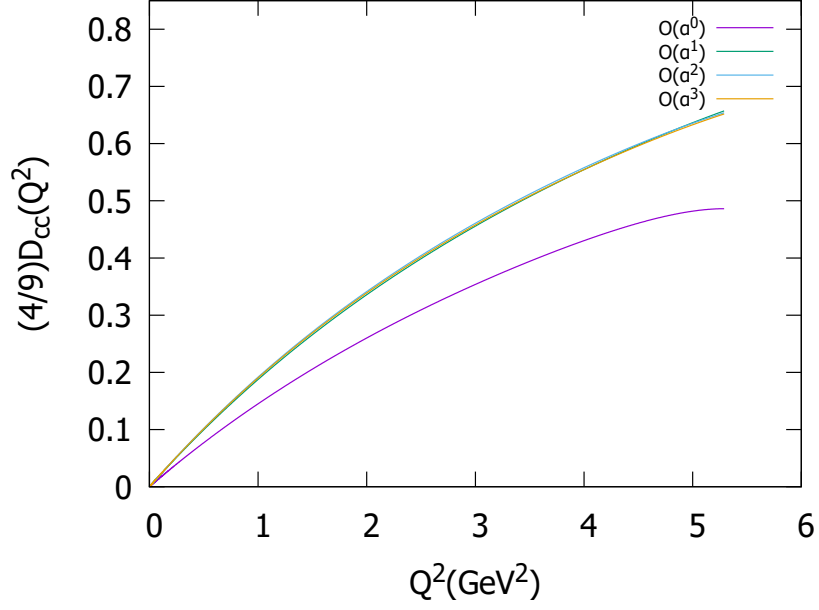


Figure 7. $D_{cc}(Q^2)$ at different orders in α_s . The input value $\alpha_s^{(n_f=5)}(M_Z^2) = 0.1184$ has been adopted.

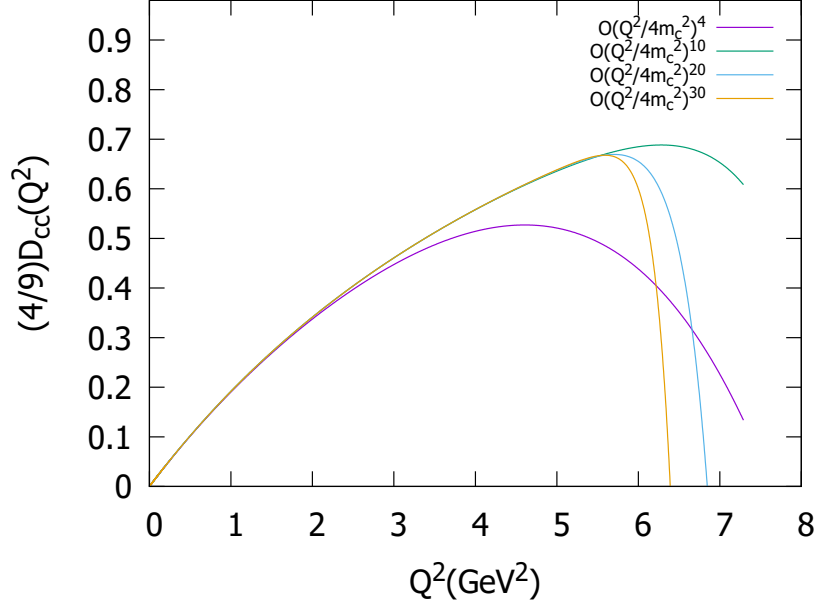


Figure 8. $D_{cc}(Q^2)$ at order α_s^2 and at different orders in the expansion of $Q^2/4m_c^2$. As expected, the convergence is better the higher the order of the expansion is. At the same time, when going beyond the radius of convergence, the higher the order the faster it goes to infinity.

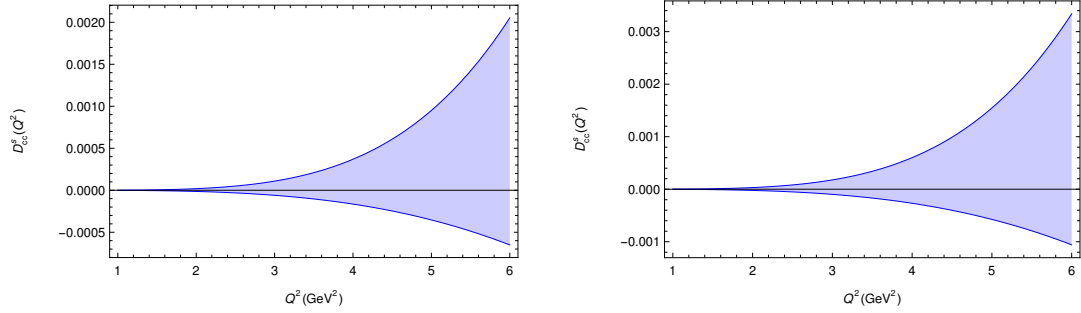


Figure 9. Estimated value of $D_{cc}^s(Q^2)$ for $\alpha_s^{(n_f=5)}(M_Z^2) = 0.115$ (left) and 0.120 (right). GeV² units.

loop corrections associated to the bottom quark are incorporated in a completely analogous way. The uncertainty of this contribution is dominated by the error on the input value of the bottom-quark mass.

3.3 QED corrections

At the precision level that we have, it is worth assessing the size of the leading QED corrections. For large Euclidean momenta, QED corrections to the Adler function can be computed perturbatively just as one computes the QCD ones.

At this level, there is a subtlety to be considered. Technically, in a full computation of the Adler function in QED plus QCD, one should incorporate the disconnected topology corresponding to a photon between two quark loops. However, this contribution is part of the vacuum polarization of the photon propagator, which, by definition, does not enter into $R(s)$. Then, consistently, at least with R-ratio data,¹⁰ we will not take that contribution into account. The remaining leading QED corrections are well known. Up to $\mathcal{O}(\alpha\alpha_s)$ [89] and heavy-quark effects, the relevant contributions can be taken into account by the following shift

$$D_{ii}^{L,(0)} \rightarrow (1 + \delta D_{ii}^{\text{QED}}) D_{ii}^{L,(0)}, \quad (3.23)$$

where

$$\delta D_{ii}^{\text{QED}} = \frac{3}{4} Q_i^2 \frac{\alpha}{\pi}. \quad (3.24)$$

Taking as central value the average between the results for $D_{ii}^{L,(0)}$ obtained at $Q = 2$ GeV with $\alpha_s = 0.1184$ and $\alpha_s = 0$ (both choices are correct up to $\mathcal{O}(\alpha\alpha_s)$ effects) and half their difference as perturbative uncertainty, one finds,

$$\Delta D_{\text{QED}}(Q^2) \equiv D(Q^2) - D^{\alpha=0}(Q^2) = 0.0012(4), \quad (3.25)$$

where the error includes a conservative estimate of missing QED corrections associated with heavy-quark loops. Perturbative QED corrections are then negligible, at the current precision level.

¹⁰In the Q^2 region we are interested in, this effect is subleading compared to the quoted uncertainties of the lattice-based evaluation, and then can also be neglected.

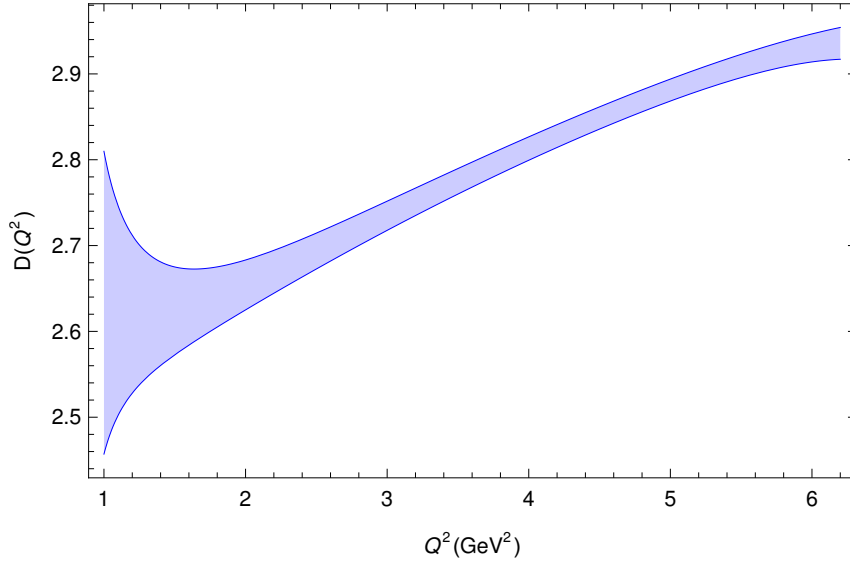


Figure 10. Final result for the perturbative $D(Q^2)$ with $\alpha_s^{(n_f=5)}(M_Z^2) = 0.1184 \pm 0.0008$ along with its uncertainty.

3.4 Compilation

We have now all the needed ingredients to build up the full perturbative Euclidean Adler function below the charm threshold. Up to negligibly small corrections, one has¹¹

$$D(Q^2) = \sum_{i,j} Q_i Q_j D_{ij}(Q^2) = \frac{2}{3} D_{ii}^{L,(0)}(Q^2) + \frac{1}{9} \Delta_{m_s} D_{33}^L(Q^2) + \frac{2}{3} D_{ii}^{L,m_c}(Q^2) + \frac{4}{9} D_{cc}(Q^2) + \frac{4}{9} D_{cc}^s(Q^2) + \frac{1}{9} D_{bb}(Q^2) + \Delta D_{\text{QED}}(Q^2). \quad (3.26)$$

In Table 3 we present our numerical results for $\alpha_s^{(n_f=5)}(M_Z^2) = (0.115, 0.120)$ and the current lattice average $\alpha_s^{(n_f=5)}(M_Z^2) = 0.1184 \pm 0.0008$ [41, 90–95] for $Q^2 = 3, 4, 5 \text{ GeV}^2$, including uncertainties.

In Fig. 10 we plot our final result for the perturbative Adler function $D(Q^2)$, including all estimated uncertainties.¹² The relative size of the different contributions and their corresponding errors are shown in Fig. 11.

4 Adler function based on the experimental ratio $R(s)$ and lattice data

In this section we discuss in some detail the experimental data that we use for $R(s)$ (based on the DHMZ compilation [24, 28]) and the lattice inputs (based on the Mainz results of

¹¹The only ones not yet discussed are the $\sum_{i=1}^3 Q_i D_{ic(b)}$ ones, which can only enter through disconnected diagrams. However, taking into account that $\sum_{i=1}^3 Q_i = 0$, they vanish in the chiral limit and then they are suppressed by $\alpha_s^3 \frac{m_s^2 Q^2}{m_{c(b)}^4}$, which makes them completely negligible.

¹²Let us note how the observed bending at $Q^2 \sim 5.5 - 6 \text{ GeV}^2$ is not a physical feature of the Euclidean Adler function, but a first signature of the breakdown of the series in powers of $\frac{Q}{2m_c}$. As a consequence we will restrict the comparisons with other determinations to $Q^2 < 5.5 \text{ GeV}^2$.

$\alpha_s^{(n_f=5)}(M_Z^2)$	Q^2	$\frac{2}{3}D_{ii}^{L,(0)}$	$\frac{1}{9}\Delta_{m_s}D_{33}^L$	$\frac{2}{3}D_{ii}^{L,m_c}$	$\frac{4}{9}D_{cc}$	$\frac{4}{9}D_{cc}^s$	$\frac{1}{9}D_{bb}$	ΔD_{QED}	D
0.115	3	2.2395(77)	-0.0123(12)	0.0039(10)	0.4484(21)(24)	0.0000(00)	0.0130(01)	0.0012(04)	2.694(09)
	4	2.2175(52)	-0.0080(07)	0.0045(12)	0.5435(24)(26)	0.0000(01)	0.0171(02)	0.0012(04)	2.776(07)
	5	2.2033(39)	-0.0058(04)	0.0050(13)	0.6197(31)(26)	0.0001(03)	0.0212(02)	0.0012(04)	2.845(06)
0.120	3	2.2866(156)	-0.0141(17)	0.0053(21)	0.4649(47)(24)	0.0000(01)	0.0132(01)	0.0012(04)	2.757(17)
	4	2.2542(98)	-0.0089(09)	0.0062(24)	0.5629(53)(26)	0.0001(02)	0.0174(02)	0.0012(04)	2.833(12)
	5	2.2343(70)	-0.0063(06)	0.0069(26)	0.6429(65)(27)	0.0002(05)	0.0215(02)	0.0012(04)	2.900(11)
0.1184(8)	3	2.2699(124)	-0.0134(15)	0.0048(17)	0.4591(36)(24)	0.0000(01)	0.0131(01)	0.0012(04)	2.735(17)
	4	2.2414(79)	-0.0086(08)	0.0055(19)	0.5561(41)(26)	0.0001(02)	0.0173(02)	0.0012(04)	2.813(14)
	5	2.2236(58)	-0.0061(05)	0.0062(20)	0.6348(51)(27)	0.0002(04)	0.0214(02)	0.0012(04)	2.881(13)

Table 3. Values of the different contributions to the Euclidean Adler function for different input values of $\alpha_s^{(n_f=5)}(M_Z^2)$. The first and second uncertainties in D_{cc} correspond, respectively, to the perturbative error and the one coming from the input charm mass. Uncertainties in α_s in the last three rows are only included for the final number, D .

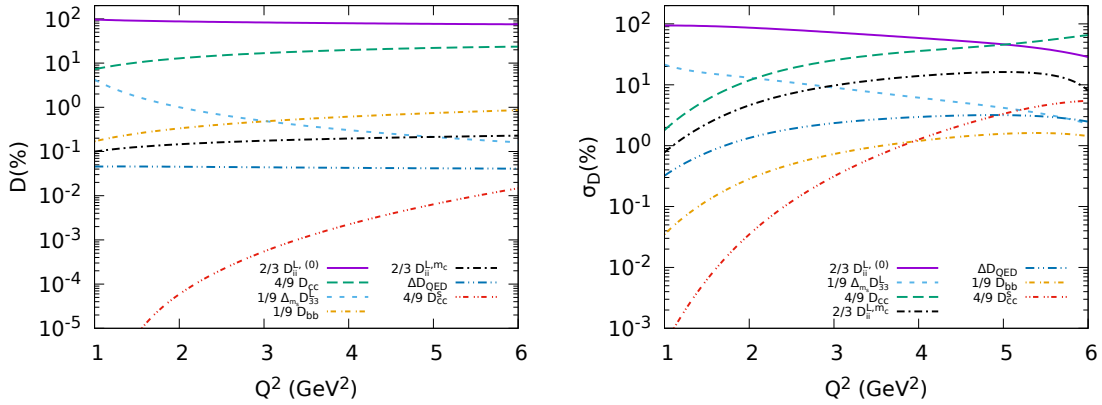


Figure 11. Relative contribution to the value (left) and the uncertainty (right) of $D(Q^2)$ as a function of Q^2 taking as input $\alpha_s^{(n_f=5)}(M_Z^2) = 0.1184$.

Ref. [14]).

4.1 Experimental ratio $R(s)$

The experimental results on $R(s)$ used in this work are based on the DHMZ data compilation made in Refs. [24, 28]. More concretely, we make use of a previous study of the different contributions to $R(s)$, performed with a full treatment of the uncertainties and their correlations. This information allows us to evaluate the hadronic running of $\alpha(Q^2)$, $\Delta\alpha_{\text{had}}(Q^2)$ (see the top panels of Fig. 12), which is then used in order to derive the Adler function with its various uncertainty components and its covariance matrix.

The Adler function emerging from the $R(s)$ data is displayed in the bottom panels of Fig. 12, together with the associated correlation matrix. The relative size of the various contributions to $D(Q^2)$ and of their corresponding uncertainties are shown in Fig. 13. At low values of Q^2 , the exclusive channels fully dominate. This contribution, corresponding to the region $\sqrt{s_{\text{th}}} < \sqrt{s} < 1.8 \text{ GeV}$, is derived based on the measurements of 32 exclusive channels. This compilation takes into account the statistical and systematic correlations between the different points/bins of a given measurement, between different experiments measuring a given channel, as well as between different channels [24, 28, 96, 97]. In this procedure, possible tensions between different measurements of a given channel are also taken into account. This is generally done in the combination, through an enhancement of the uncertainties by a factor $\sqrt{\chi^2/\text{ndof}}$, applied in all the \sqrt{s} bins where this factor is larger than unity. In addition, an extra uncertainty accounting for the systematic deviations between the BaBar [98, 99] and KLOE [100–102] measurements in the 2π channel has been included for the first time in Ref. [28], by comparing the combination results obtained when excluding either of the two experiments.¹³ This uncertainty turns out to be dominant in

¹³Note: Recently, a new precise measurement of the 2π channel performed by the CMD-3 collaboration has been made public [103]. In the dominant ρ -resonance region, it features larger cross-section values compared to all previous experiments, in particular the most precise ones from BaBar [98, 99] and KLOE [100–102].

the case of the theoretical prediction for the anomalous magnetic moment of the muon, hence the importance of fully taking this systematic effect into account. The remaining data-based contributions come from the $3.7 \text{ GeV} < \sqrt{s} < 5 \text{ GeV}$ interval, the dispersive integrals being evaluated based on the inclusive measurements available in this range, and from the narrow J/Ψ and $\Psi(2S)$ resonances.

Unfortunately, no precise enough data are yet available for the remaining regions, $1.8 \text{ GeV} < \sqrt{s} < 3.7 \text{ GeV}$ ¹⁴ and $\sqrt{s} > 5 \text{ GeV}$, and there one needs to rely on perturbation theory for $R(s)$.¹⁵ This happens to be a more critical and limiting factor for the associated Adler function, especially at large Q^2 , where this contribution eventually dominates when $Q \gtrsim 2 \text{ GeV}$.

4.2 Lattice Adler function

The study about the hadronic running of the electromagnetic coupling from lattice QCD presented in Ref. [14] contains all the needed details to extract the corresponding Adler function together with estimated uncertainties and correlations. In order to be able to keep track of them, we use the rational approximation for $\bar{\Pi}(Q^2)$ presented in that reference:

$$\bar{\Pi}(Q^2) \approx \frac{\sum_{n=1}^3 a_n x^n}{1 + \sum_{n=1}^3 b_n x^n} = \frac{0.1094(23)x + 0.093(15)x^2 + 0.0039(6)x^3}{1 + 2.85(22)x + 1.03(19)x^2 + 0.0166(12)x^3}, \quad (4.1)$$

where $x \equiv Q^2/\text{GeV}^2$ and the correlation matrix of the expansion coefficients is given by

$$\text{corr} \begin{pmatrix} a_1 \\ a_2 \\ a_3 \\ b_1 \\ b_2 \\ b_3 \end{pmatrix} = \begin{pmatrix} 1 & & & & & \\ 0.455 & 1 & & & & \\ 0.17 & 0.823 & 1 & & & \\ 0.641 & 0.946 & 0.642 & 1 & & \\ 0.351 & 0.977 & 0.915 & 0.869 & 1 & \\ 0.0489 & -0.0934 & 0.0667 & -0.044 & -0.115 & 1 \end{pmatrix}. \quad (4.2)$$

It is worth noticing that, when comparing the rational approximation of $\bar{\Pi}(Q^2)$ with the tables of that reference, we observe that, while this approximation gives a very accurate description of the central value up to $Q^2 \sim 7 \text{ GeV}^2$, a significant reduction of the uncertainties (up to 50%) starts appearing at 2 GeV^2 , due to a more conservative treatment of discretization effects and, to some extent, to the constraint due to the assumed rational approximation ansatz.

We obtain the corresponding lattice Adler function by simply using Eqs. (2.1) and (2.2). The result is displayed in Fig. 14.

While dispersive integrals computed with these new inputs are certainly enhanced and closer to the ones obtained from Lattice QCD, it is of utmost importance to first achieve a better understanding of the tensions on the experimental side. In particular, one needs to understand the source of tension between the CMD-3 results and the former CMD-2 measurements [104, 105], performed in somewhat similar conditions by the same group.

¹⁴The relatively precise BES III and KEDR results are in tension in the range $3.40 \text{ GeV} < \sqrt{s} < 3.67 \text{ GeV}$ [106].

¹⁵Notice, however, that the perturbative uncertainties include also the estimated size of potential violations of quark-hadron duality in the region $1.8 - 2 \text{ GeV}$ [28].

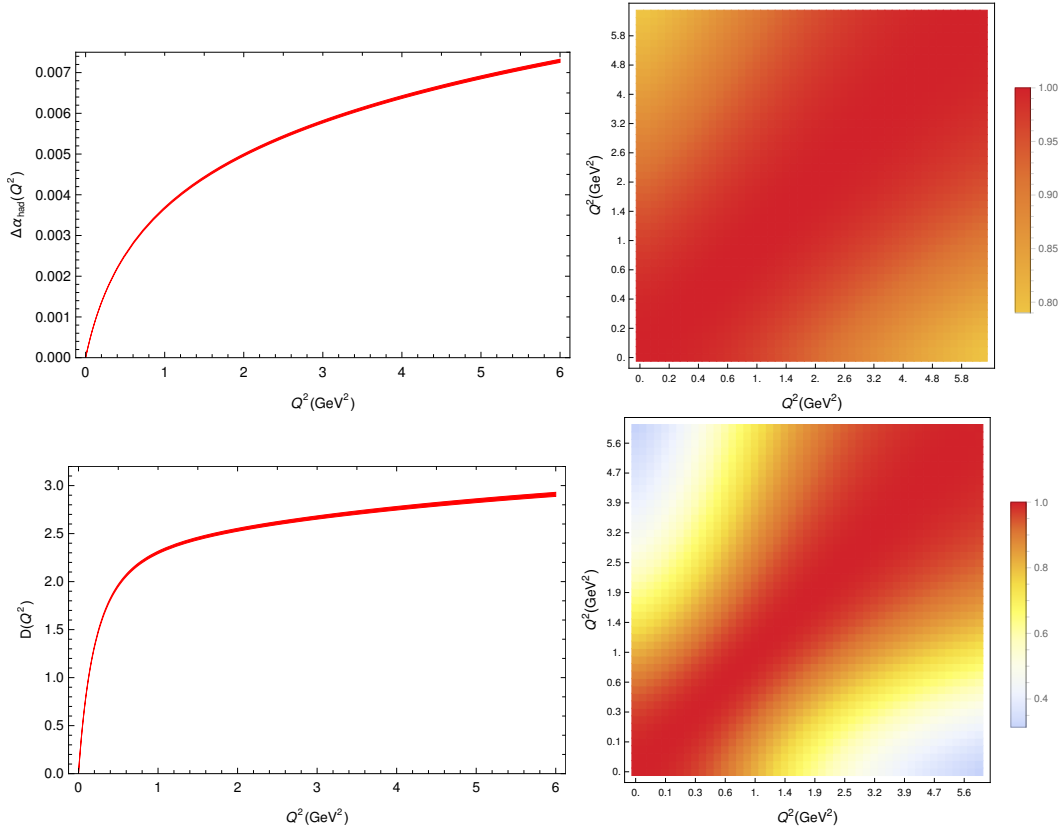


Figure 12. Results for $\Delta\alpha_{\text{had}}(Q^2)$ (top) and $D(Q^2)$ (bottom) from the data-driven dispersive evaluation based on the ratio $R(s)$, together with their correlations (right). The half-width of the red band indicates the total uncertainty.

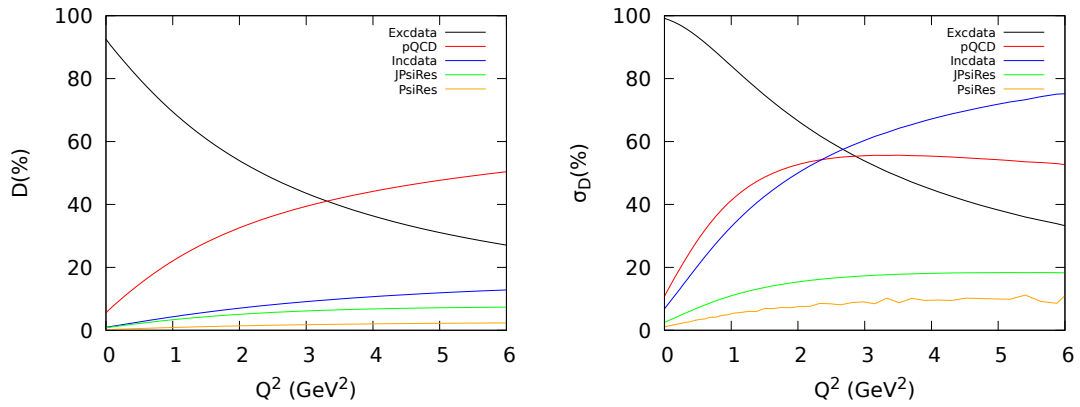


Figure 13. Relative size of the different contributions to $D(Q^2)$ (left) and to their uncertainties (right) entering the data-driven dispersive evaluation based on the R-ratio.

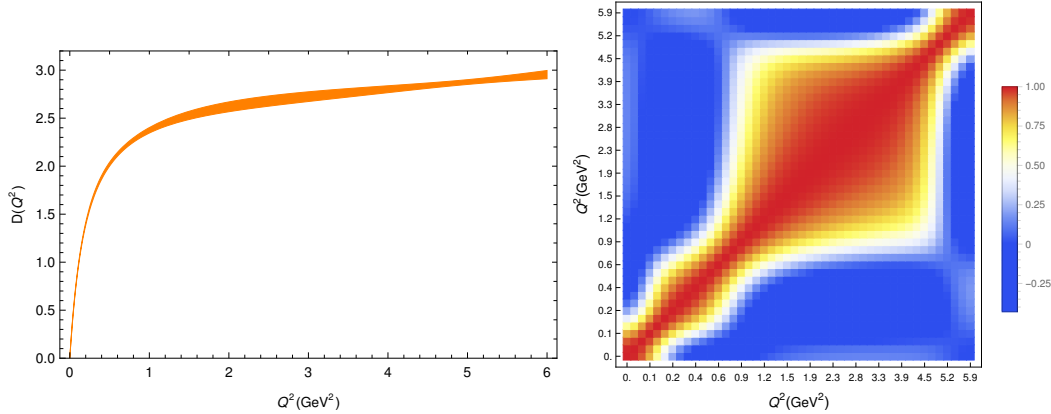


Figure 14. Adler function obtained from the lattice results of Ref. [14] (left) together with its correlation matrix (right).

5 Comparison of the three different approaches to $D(Q^2)$

We can finally perform the comparison of the three descriptions of the Adler function. For the perturbative one we will take the same inputs as above *i.e.* $\alpha_s^{(n_f=5)}(M_Z^2) = 0.1184 \pm 0.0008$, $m_s(\mu_0^2) = (92.03 \pm 0.88)$ MeV at $\mu_0 = 2$ GeV, $m_c(m_c^2) = 1.275$ (5) GeV and $m_b(m_b^2) = 4.171$ (20) GeV from the FLAG lattice review [41, 42, 42–54, 66–70, 90–95, 107]. The results are presented in Fig. 15. In Fig. 16 we quantify the tension among the different descriptions of the Adler function in terms of the statistical significance of their differences, *i.e.*

$$S^{ij}(Q^2) \equiv \frac{D^i(Q^2) - D^j(Q^2)}{\sigma_{[D^i(Q^2) - D^j(Q^2)]}}, \quad (i, j = \text{pQCD}, e^+e^- \text{ data, latt}). \quad (5.1)$$

We observe the following:

1. The estimate based on e^+e^- data has smaller uncertainties than the lattice determination. The quoted pQCD precision becomes competitive at $2 - 3$ GeV².
2. In the whole energy range analysed, the lattice determination of $D(Q^2)$ has a larger central value than the one inferred from e^+e^- data. This follows the same trend as in $g - 2$ and $\Delta\alpha_{\text{had}}$. However, within the quoted uncertainties, these two estimates of the Adler function remain compatible at large values of Q^2 , the statistical significance of their difference being $\sim 1\sigma$.
3. The lattice determination is in excellent agreement with pQCD in the region where perturbation theory is reliable, *i.e.* at $Q^2 \gtrsim 2 - 4$ GeV². The differences between the two determinations (central values) is only $\sim 0.2\sigma$. Some tension, larger than 1σ , is observed at lower values of Q^2 . This is expected, both because systematic perturbative uncertainties become less reliable and because power corrections are expected to emerge.

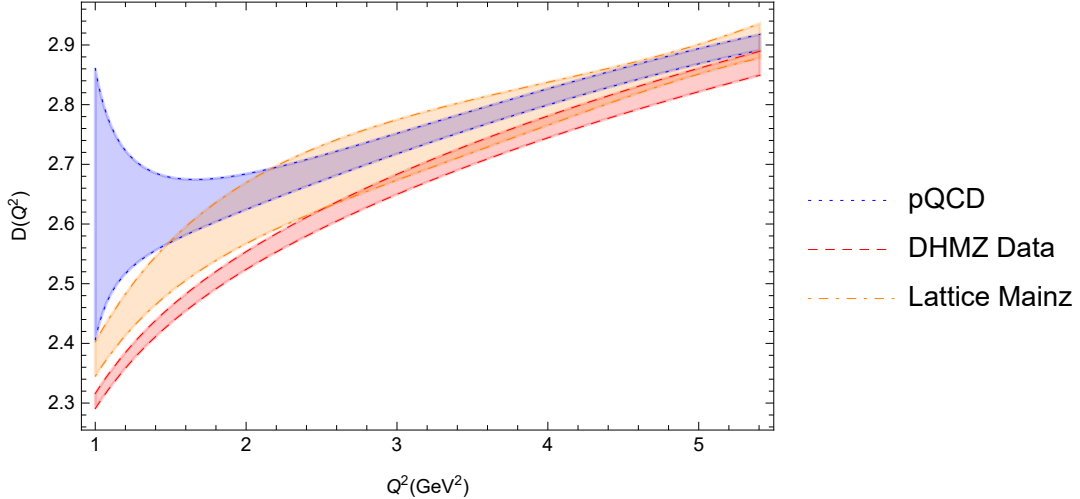


Figure 15. Comparison between the Adler functions obtained from pQCD, the DHMZ compilation of e^+e^- data and the lattice results of Ref. [14].

4. A significant tension between the determinations of $D(s)$ from e^+e^- data and pQCD emerges below 5 GeV^2 . It is larger than 2σ , and it even surpasses 3σ at $Q^2 \sim 1.5 - 3 \text{ GeV}^2$. Let us give three possible explanations for it. First, at low Q^2 values, power corrections can become sizeable and may explain the discrepancy. We analyze this possibility in more detail in the next section. The second possibility is that the strong coupling is lower than the value used as an input. From that perspective one can translate this tension into a tension between the value of α_s obtained from a fit to e^+e^- data and the lattice average that we are using as input. We will study this perspective in more detail below. New precise results from novel methods agreeing with the lattice average [108] suggest that such a large disagreement is unlikely. The third possible explanation for the tension at large Q^2 values, appears to be possible unaccounted systematic effects in the dispersive evaluation of the Adler function (see Fig. 13 for the various contributions to this evaluation and to its uncertainty).

6 Nonperturbative corrections to the perturbative Adler function

We aim to assess up to which level power corrections can account for the deviations observed in the previous section between the Adler function emerging from e^+e^- data and pQCD. This is not straightforward because the needed vacuum expectation values are not known from first principles and, in general, their numerical values can depend on the way one truncates the (asymptotic) perturbative series.

In fact, the factorial growth of the perturbative expansion at large orders generates infrared ambiguities (when one tries to reconstruct the Adler function from its Borel sum) that scale as inverse powers of Q^2 and are expected to be reabsorbed into the nonperturbative terms of the OPE. One may be tempted to state that those effects are already accounted

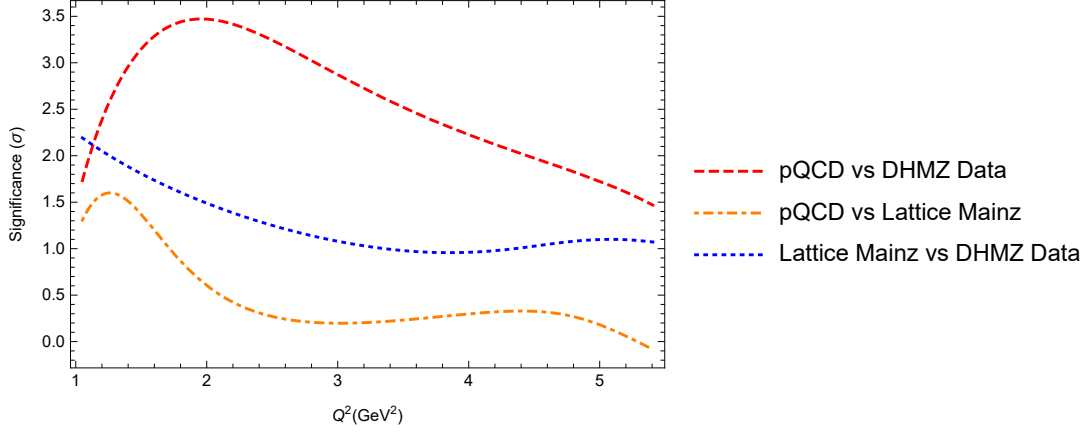


Figure 16. Statistical significance of the differences between the three determinations of the Adler function.

for in the perturbative systematic uncertainties. However, the existence of vacuum matrix elements is well established beyond perturbation theory [2, 3]. The nonperturbative nature of the QCD vacuum generates non-zero vacuum expectation values for many composite operators such as the quark condensate $\langle 0|\bar{q}q|0\rangle$, responsible for the breaking of chiral symmetry, or the gluon condensate $\langle 0|a_s G_{\mu\nu} G^{\mu\nu}|0\rangle$, which breaks the scale invariance of massless QCD.

Pure nonperturbative observables, where perturbation theory vanishes, allow for cleaner determinations of the corresponding vacuum condensates because their numerical effects cannot be masked by perturbative uncertainties. This is the case of the two-point function of a left-handed and a right-handed currents (the $VV - AA$ correlator), which is identically zero to all perturbative orders in α_s but receives non-zero contributions from $D \geq 6$ vacuum condensates that are order parameters of the chiral symmetry breaking. The sizes of the leading power corrections to this correlator are well known, since they can be directly extracted from the τ decay data [109, 110]. Since there is no reason to neglect them, neither in the vector correlator nor in the axial one, it is then a must to incorporate power corrections for a complete description of the OPE-based Adler function.

6.1 Light-quark correlators

The leading nonperturbative contribution to the Adler function is, up to negligible up and down quark-mass corrections [9, 36],

$$\delta D_{ii}^{L,D=4} = \frac{2\pi^2}{Q^4} \left\{ \left(1 + \frac{7}{6} a_s \right) \langle a_s GG \rangle + 24 m_s \langle \bar{s}s \rangle \left[\delta_{i3} \left(1 + \frac{a_s}{3} + \frac{47}{8} a_s^2 \right) + (8\zeta_3 - 5) \frac{a_s^2}{12} \right] \right\}, \quad (6.1)$$

which implies for the total electromagnetic correlator:

$$\delta D_{\text{em}}^{L,D=4} = \frac{4\pi^2}{3Q^4} \left\{ \left(1 + \frac{7}{6} a_s \right) \langle a_s GG \rangle + 4 \left[1 + \frac{a_s}{3} + \left(\frac{27}{8} + 4\zeta_3 \right) a_s^2 \right] m_s \langle \bar{s}s \rangle \right\}. \quad (6.2)$$

The numerical value of the gluon condensate is quite uncertain [111, 112], since it is difficult to separate its effect from the ambiguity generated by the asymptotic tail of the

perturbative series, which is supposed to be already included in the perturbative uncertainty. On the other hand, from general grounds we know that the gluon condensate is positively defined [2]. This is an important point, because it actually means that its corresponding $D = 4$ power correction goes into the wrong direction to explain the tension between pQCD and the experimental data on $R(s)$. To be on the conservative side, let us take the central value estimated in Ref. [2], but with a 100% of uncertainty, *i.e.*

$$\left\langle \frac{\alpha_s}{\pi} GG \right\rangle = (0.012 \pm 0.012) \text{ GeV}^4. \quad (6.3)$$

The strange quark condensate is better known because it is related to the kaon mass and decay constant by chiral symmetry [113]. Since it is an order parameter of the chiral symmetry breaking (it vanishes to all orders in perturbation theory), the quark condensate does not suffer from the perturbative ambiguity mentioned before. At lowest-order in chiral perturbation theory it gets determined by the old Gell-Mann–Oakes–Renner relation [114]. However, it receives large higher-order corrections that enhance its final uncertainty [115–117]:

$$m_s \langle \bar{s}s \rangle = -F_K^2 M_K^2 \left[1 - \delta_{\mathcal{O}(p^4, m_{u,d})} \right] \approx -(1.3 \pm 0.7) \cdot 10^{-3} \text{ GeV}^4. \quad (6.4)$$

The combined dimension-four correction to the electromagnetic Adler correlator in Eq. (6.2) takes then the value:

$$\delta D_{\text{em}}^{L,D=4} \approx \frac{(0.10 \pm 0.18) \text{ GeV}^4}{Q^4}. \quad (6.5)$$

Let us also account for the $D = 6$ contribution. Up to residual pieces that vanish in the electromagnetic sum, one can write the $D = 6$ contribution as

$$\Pi_{ii}^{L,D=6} = \frac{\mathcal{O}_{6,V}}{Q^6}. \quad (6.6)$$

It is convenient to rewrite

$$\mathcal{O}_{6,V} = \frac{1}{2} (\mathcal{O}_{6,V-A} + \mathcal{O}_{6,V+A}). \quad (6.7)$$

The $\mathcal{O}_{6,V-A}$ contribution is a genuine vacuum condensate whose nonzero value, $\mathcal{O}_{6,V-A} \approx -0.0035(9) \text{ GeV}^6$ [109], is well established and understood beyond perturbation theory, and its effect is unrelated to the perturbative series, which is identical for the vector and axial channels. Nonperturbative effects in the observed spectrum (see for example [118, 119]) are known to be suppressed for the $V + A$ combination with respect to the $V - A$, which motivates to assume $|\mathcal{O}_{6,V+A}| < |\mathcal{O}_{6,V-A}|$ [120]. This inequality holds (by far) in the large- N_C limit, which gives $\mathcal{O}_{6,V+A}^\infty = -\frac{2}{9} \mathcal{O}_{6,V-A}^\infty$, reproducing the old vacuum saturation approximation, which is also known to work well in predicting $\mathcal{O}_{6,V-A}$ and some rigorous inequalities [2]. Taking this into account, we will adopt

$$\mathcal{O}_{6,V} = (-0.0015 \pm 0.0015) \text{ GeV}^6, \quad (6.8)$$

as an estimate of this contribution. For the needed Adler function one finds

$$D_{\text{em}}^{L,D=6} \approx 24\pi^2 \frac{\mathcal{O}_{6,V}}{Q^6} = \frac{-(0.36 \pm 0.36) \text{ GeV}^6}{Q^6}. \quad (6.9)$$

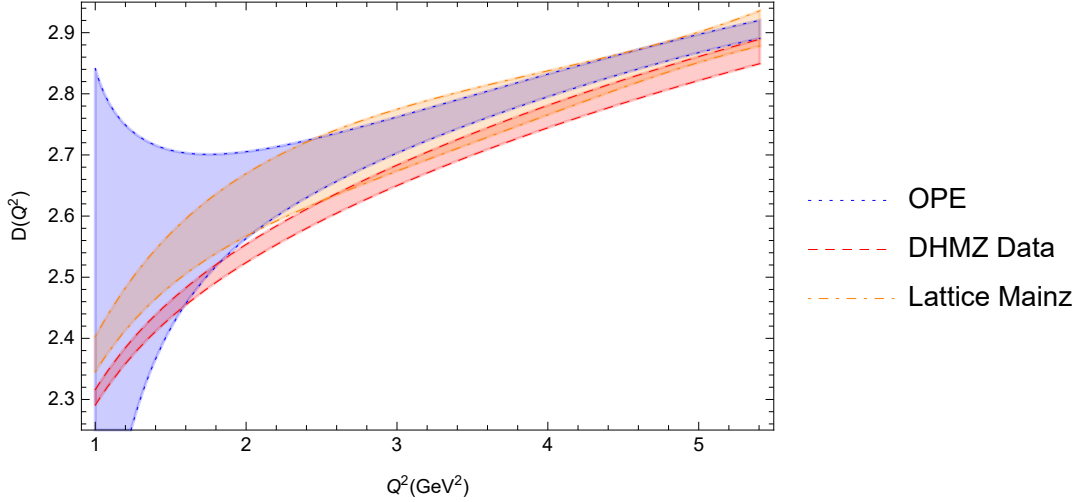


Figure 17. Same plot as Fig. 15 but including the nonperturbative contribution in Eq. (6.12).

Notice that the assigned uncertainties to those corrections potentially contaminated by perturbation theory (gluon condensate and $\mathcal{O}_{6,V+A}$) are above 100% of their corresponding estimates, guaranteeing that any potential double-counting effect is consistently absorbed by our conservative errors.

6.2 Charm correlator

Much less relevant for our analysis is the contribution of power corrections to the charm correlator. The leading power correction is given by the gluon condensate contribution [2]:

$$D_{cc}(Q^2) = -12\pi^2 Q^2 \frac{d}{dQ^2} \left[\frac{\langle \frac{\alpha_s}{\pi} GG \rangle}{4 \cdot 12 Q^4} F \left(1 + \frac{4m_c^2}{Q^2} \right) \right], \quad (6.10)$$

where

$$F(a) \equiv \frac{3(a+1)(a-1)^2}{a^2} \frac{1}{2\sqrt{a}} \ln \left(\frac{\sqrt{a}+1}{\sqrt{a}-1} \right) - \frac{3a^2 - 2a + 3}{a^2}. \quad (6.11)$$

Taking again $\langle a_s GG \rangle = (0.012 \pm 0.012) \text{ GeV}^2$, one can easily check that the contribution to $D(Q^2)$ remains below 10^{-3} and can then be neglected.

6.3 Discussion

The nonperturbative correction to the Adler function is then given by

$$\delta D_{\text{em}}^{\text{NP}} \approx \frac{4\pi^2}{3Q^4} \left\{ \left(1 + \frac{7}{6} a_s \right) \langle a_s GG \rangle + 4 \left[1 + \frac{a_s}{3} + \left(\frac{27}{8} + 4\zeta_3 \right) a_s^2 \right] m_s \langle \bar{s}s \rangle \right\} + 24\pi^2 \frac{\mathcal{O}_{6,V}}{Q^6}. \quad (6.12)$$

Adopting the conservative numerical estimates in Eqs. (6.3), (6.4) and (6.8), we find that the nonperturbative uncertainty is actually larger than the perturbative one at low Q^2 values and, at the current precision level, it cannot be fully neglected even at $Q^2 \approx 4 \text{ GeV}^2$. We show in Fig. 17 the comparison of the OPE (pQCD plus condensates) Adler function

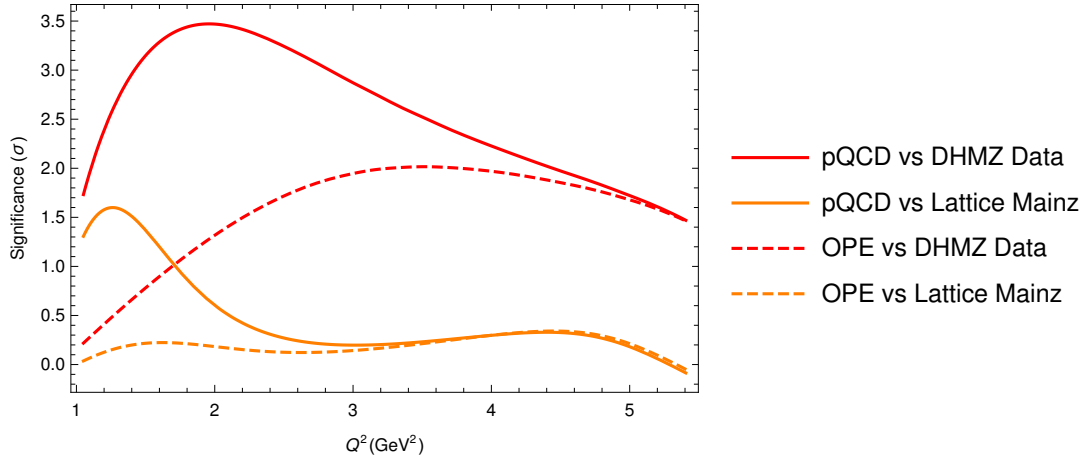


Figure 18. Statistical significance of the difference between the Adler functions extracted from e^+e^- data and lattice results with respect to both the OPE and pQCD predictions.

with the other approaches, and in Fig. 18 the statistical significance of the differences with respect to the lattice and e^+e^- -data evaluations of the Adler function. We observe that the origin of the tension at $\sim 1 \text{ GeV}^2$ between the perturbative prediction and both lattice and DHMZ results can indeed be explained by genuine nonperturbative effects. Incidentally, the input central values assumed for the vacuum condensates fit very well the shape of the distribution, although slightly different estimates cannot be discarded within the current experimental and lattice uncertainties, also depending on the size of higher-order power corrections. On the other hand, for $Q^2 \gtrsim 2 \text{ GeV}^2$, the observed tension between the analytic Adler function and the data-based one gets slightly reduced. This reduction decreases with Q^2 , as the effect of the nonperturbative terms diminish, and a tension of up to $\sim 2\sigma$ remains.

7 Determination of α_s from the Adler function

Instead of using α_s as input to compare the perturbative $D(Q^2)$ with the other approaches, we can reconvert the comparison into an α_s extraction. The extraction can be done at each value of Q^2 by solving the equation:

$$D^{\text{OPE}}(Q^2, \alpha_s) - D^{\text{data}}(Q^2) = 0, \quad (7.1)$$

for α_s while keeping Q^2 fixed. $D^{\text{OPE}}(Q^2, \alpha_s)$ is the sum of the perturbative and nonperturbative contributions of the theoretical Adler function, Eqs. (3.26) and (6.12), keeping α_s as a variable. $D^{\text{data}}(Q^2)$ is the Adler function obtained through either the experimental ratio $R(s)$, $D^{R(s)}(Q^2)$, or the lattice data, $D^{\text{latt}}(Q^2)$, which were discussed in Sec. 4. In this section we illustrate the procedure by using the Adler function based on $R(s)$. The results for the analogous lattice fits are relegated to App. C.¹⁶

¹⁶Notice however how lattice data is not limited to the full EM correlator and then better strategies to extract α_s can in principle be pursued.

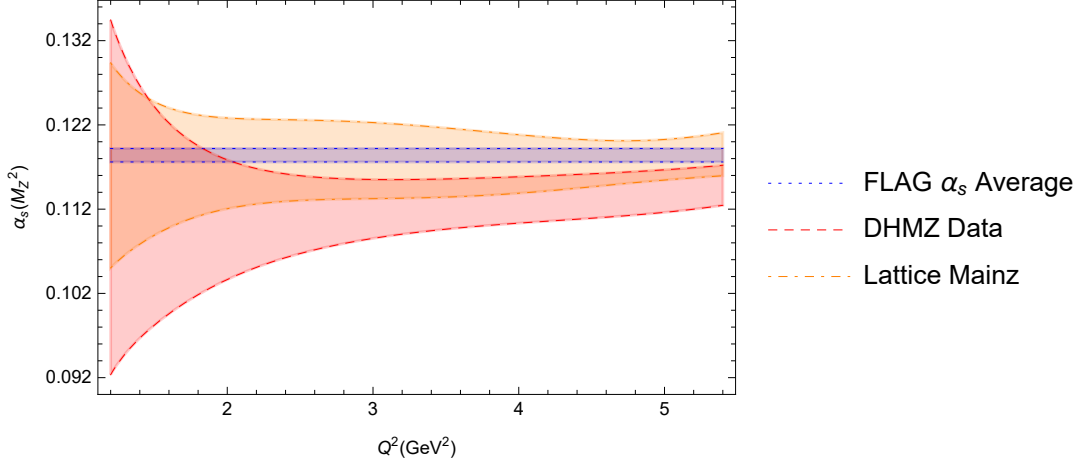


Figure 19. Comparison between the lattice FLAG average $\alpha_s^{(n_f=5)}(M_Z^2) = 0.1184 \pm 0.0008$ and the values of α_s obtained at each Q^2 for the $R(s)$ and lattice Adler functions.

As explained in Sec. 4, the $R(s)$ data relies on perturbation theory for the regions $1.8 \text{ GeV} < \sqrt{s} < 3.7 \text{ GeV}$ and $\sqrt{s} > 5 \text{ GeV}$. This means that the $R(s)$ -based Adler function also contains a residual dependence on α_s , which we take into account in the extraction. We decompose $D^{R(s)}$ into the sum of two contributions: one coming from experimentally measured values, $D_{\text{exp}}^{R(s)}(Q^2)$ (see Fig. 13), and one corresponding with the perturbation theory contribution, $D_P^{R(s)}(Q^2, \alpha_s)$. The resulting equation to solve for α_s at each Q^2 becomes:

$$D^{\text{OPE}}(Q^2, \alpha_s) - (D_{\text{exp}}^{R(s)}(Q^2) + D_P^{R(s)}(Q^2, \alpha_s)) = 0. \quad (7.2)$$

The values for $\alpha_s^{(n_f=5)}(M_Z^2)$ obtained from both lattice and $R(s)$ data, together with their uncertainties, including both all experimental and theoretical sources, are plotted in Fig. 19, as a function of the Q^2 value at which they are derived. As expected, the same observations made when comparing the different Adler functions are applicable here as well. That is,

1. The central values of the strong coupling extracted from e^+e^- data are smaller than the ones extracted using the lattice determination of $D(Q^2)$.
2. The values of α_s extracted from lattice data are in agreement with the FLAG lattice average.
3. The α_s extracted from e^+e^- data is between 1.5 and 2σ below the FLAG lattice average in the $3 \text{ GeV}^2 < Q^2 < 5 \text{ GeV}^2$ region. Notice however how the different Q^2 points are strongly correlated among each other.

In the following, we discuss how these different values for α_s can be compared quantitatively and combined.

7.1 Averages

A potential improvement in terms of precision for the extracted $\alpha_s^{(n_f=5)}(M_Z^2)$ could come from combining the values obtained at different Q^2 values, taking into account their correlations. One possibility would be to perform the combination through the minimisation of a χ^2 function,

$$\chi^2 = (\bar{\alpha}_s^{\text{extr}} - \bar{\alpha}_s^{\text{av}}) \cdot C^{-1} \cdot (\bar{\alpha}_s^{\text{extr}} - \bar{\alpha}_s^{\text{av}})^T, \quad (7.3)$$

with respect to α_s^{av} . In this function, $\bar{\alpha}_s^{\text{extr}}$ is the vector containing the extracted values of α_s at each Q^2 , C is their covariance matrix¹⁷ and $\bar{\alpha}_s^{\text{av}}$ is a vector with the same dimension as $\bar{\alpha}_s^{\text{extr}}$ containing the parameter α_s^{av} . However, one is faced with the following limitations:

1. As discussed in the previous section, the nonperturbative contributions to the Adler function are a large source of systematic uncertainty at low Q^2 , which additionally is not fully controlled. This can clearly be seen in Fig. 19. Therefore, one should avoid using the extracted values in this energy region.
2. The values extracted from e^+e^- data display strong experimental correlations (see Fig. 12). These correlations are stronger between neighboring points and a larger precision in the estimation of the corresponding covariance matrix would be needed in order to find meaningful results for the combination, which may otherwise not be realistic. Indeed, if one includes too many consecutive points, eventually one is going to find a covariance matrix with null eigenvalues, which would imply absolute predictions (*i.e.* no uncertainties in certain linear combinations). Actually, this is a consequence of the approximations involved in finding the original covariance matrix.¹⁸ Additionally this makes the experimental correlation matrix singular, which therefore cannot be inverted. As a result, a χ^2 function cannot be constructed for the whole set of extracted values.
3. A similar problem arises for the theoretical correlation matrix. In general one expects that the perturbative uncertainties are dominated by the first unknown coefficient, in this case K_5 , and the nonperturbative ones by the first unknown power correction, say \mathcal{O}_6 . We have supplemented the perturbative uncertainty by renormalization-scale variations, which in general one expects to account for uncertainties due to higher-order effects. However this is going to fail if one artificially looks for linear combinations of data points such that either K_5 , \mathcal{O}_6 and/or the scale variations cancel or they appear suppressed, for example by numerical prefactors, with respect

¹⁷In principle, for e.g. relative uncertainties, this covariance matrix can itself depend on α_s^{av} , which could be addressed through an iterative fitting approach (see e.g. Refs.[121, 122] and references therein) or using fitted nuisance parameters applied as (constrained) scaling factors of the theoretical prediction [123, 124]. However, here the input α_s^{extr} values are similar (see e.g. Fig. 19) and the impact of this effect is small.

¹⁸An illustrative example of this (extreme) case, this time for fit inputs from lattice QCD, would consist in simply starting from Eq. (4.1) and taking 7 different points. While the rational approximation and their associated uncertainties are expected to work generally well both in $\bar{\Pi}(Q^2)$ and linear combinations of it, it would clearly fail in predicting the uncertainties of the linear combination corresponding to the zero eigenvalue (corresponding to a null estimated uncertainty), which would directly dominate (because of an apparently infinite precision) the determination of any theoretical parameter depending on it.

to the contributions of higher-order coefficients, which then by construction are not going to be negligible with respect to the accounted effects. In a naive χ^2 fit, the extracted value of α_s is going to be dominated by the most precise linear combination of data points, taking into account those theoretical uncertainties, which are precisely the directions where the estimators are prone to underestimate them, leading to very aggressive predictions. An explicit example of this kind of direction is the logarithmic derivative of the Adler function, implicit in fits to consecutive data points.¹⁹ Indeed by taking consecutive (adimensionalized) derivatives one is going to trigger the sooner breakdown of the OPE. Schematically, for the nonperturbative contributions to D , D_{NP} , one has²⁰

$$D_{\text{NP}} \sim \sum_D c_D \frac{\Lambda^D}{Q^D} \quad \longrightarrow \quad \frac{d^n D_{\text{NP}}}{d \ln Q^n} = \sum_D c_D (-D)^n \frac{\Lambda^D}{Q^D}, \quad (7.4)$$

and then higher-dimensional corrections become more and more important with respect to lower-dimensional ones at a fixed energy, eventually leading to potentially underestimated theoretical uncertainties in those directions. Analogously, the scale variation is going to be in general a good estimator of perturbative uncertainties, because its variation is in general of the same order as the neglected perturbative contributions. However, one would clearly fall into one version of the well-known look-elsewhere effect if one artificially looks for directions in which it happens to cancel: the fact that the scale-dependence accidentally cancels in some linear combination does not guarantee that the contributions from higher-order coefficients are also cancelling. There is also the possibility that new topologies emerge at higher orders, inducing an uncertainty not well accounted by the scale variations.

In summary, the χ^2 function defined in Eq. (7.3) and the result of its minimisation are sensitive to uncertainties on the uncertainties and on the correlations (*i.e.* to uncertainties on the covariance matrix), present for both the experimental and the theoretical components. Starting from remarks made in the context of ATLAS jet performance and cross-section studies [125–127], the relevance of the uncertainties on the covariance matrices (in particular for what concerns the implications for combination methods) has been pointed out in the context of the theoretical predictions for the anomalous magnetic of the muon [28, 128, 129]. More recently, similar remarks about the uncertainties on uncertainties were made for what concerns the procedure of quantifying the significance of the data-theory tensions, in this same context [130].

Taking all these aspects into account, we will restrict to data sets with at most three points and $Q^2 \gtrsim 3 \text{ GeV}^2$. We will consider the two sets of three Q^2 points shown in Table 4. The first set, set 1, has a better behaviour in the expansion in powers of Q^2/m_c^2 , whereas

¹⁹In fact we find that the eigenvectors associated to the lowest eigenvalues of the experimental covariance matrix correspond, in first approximation, to the highest-order derivatives in the discrete approximation. They can be related to different, more localized, weights when integrating $R(s)$.

²⁰An analogous issue occurs for the $\left(\frac{Q^2}{4m_c^2}\right)^n$ series, possibly inducing the breakdown of the associated expansion from lower energies for high-order derivatives.

	Q^2	$\alpha_s(M_Z^2)$
Set 1	3.15	0.1122 (17) _{exp} (11) _{pert} (26) _{th}
	4.10	0.1132 (19) _{exp} (12) _{pert} (16) _{th}
	5.18	0.1144 (19) _{exp} (11) _{pert} (10) _{th}
Set 2	4.10	0.1132 (19) _{exp} (12) _{pert} (16) _{th}
	4.63	0.1138 (20) _{exp} (12) _{pert} (12) _{th}
	5.41	0.1148 (19) _{exp} (11) _{pert} (10) _{th}

Table 4. The two sets of three Q^2 points chosen for the averages with their experimental (exp), perturbative (pert) and theoretical (th) symmetrized uncertainties. By perturbative uncertainty we mean the uncertainty coming from the use of perturbation theory in the regions $1.8 \text{ GeV} < \sqrt{s} < 3.7 \text{ GeV}$ and $\sqrt{s} > 5 \text{ GeV}$ for the ratio $R(s)$.

the second set, set 2, is less affected by potential nonperturbative effects. Additionally we will also consider two variations with only two Q^2 values, set 1* and set 2*, where the midpoint of the corresponding set has been removed.

The only remaining input necessary to compute the χ^2 is the covariance matrix C . In order to evaluate it, we can use linear error propagation, for both the experimental and theoretical components of this matrix. In particular, for the theoretical component this is justified, since the Adler function is an approximately linear function of α_s in the energy region we are considering. However, there are different possible choices aimed to avoid the issues mentioned above when assigning correlations between the theoretical uncertainties at different points. We will explore the different possibilities in Sec. 7.2.

When performing such combination, we must also take into account the possibility of the χ^2 minimisation yielding a biased result, caused by the limited precision with which the covariance matrix is known. According to the Gauss-Markov Theorem, the minimisation of the χ^2 in Eq. (7.3) is equivalent to performing a weighted average, while optimizing the weights (constraint to have the sum equal unity) such that the uncertainty of the average is minimum [131, 132]. This yields

$$\alpha_s^{\text{av}} = \frac{\bar{\mathbf{1}} \cdot C^{-1} \cdot (\bar{\alpha}_s^{\text{extr}})^T}{\bar{\mathbf{1}} \cdot C^{-1} \cdot \bar{\mathbf{1}}^T}, \quad (7.5)$$

with $\bar{\mathbf{1}}$ being a vector of the same dimension as $\bar{\alpha}_s^{\text{extr}}$, with all its entries equal to 1. As a consequence, if the covariance matrix is poorly known, these weights can be biased (in some cases they can e.g. take negative values or values larger than unity, which could make the average value to be outside the range of the extracted values). Therefore, we have to consider alternative averaging procedures that, although will yield results with somewhat larger uncertainties (see Sec. 7.3), are free of any bias caused by implicit assumptions in the derivation of their weights. We have considered the following:

1. A simple average, where all the inputs have the same weight. This is, the inverse of the number of input values considered.

2. A weighted average where the weights are proportional to the inverse of the experimental uncertainty squared.²¹

The averaged values obtained using these different averaging procedures for the four sets considered can be found in Sec. 7.3.

7.2 Theoretical uncertainties

As discussed throughout the text, there are different sources of theoretical uncertainty to the Adler function and for some of them assigning a 100% correlation between different Q^2 values may not be the best choice. This is for example the case of the scale variations (it is probably not realistic to assume that there is a single renormalization-scale choice such that the perturbative uncertainties of all truncated series can be removed) or the nonperturbative one parameterized by \mathcal{O}_6 (knowledge of \mathcal{O}_6 would not completely remove the nonperturbative uncertainty, since we would need to account for the higher-dimensional contributions). We will then repeat the same fits under four assumptions on the correlations between the theoretical uncertainties at different Q^2 :

1. All correlations for the same “theoretical source”, renormalization scales or \mathcal{O}_6 , are 100%.
2. All correlations for the same “theoretical source” are 100% except for the scale variations, that are assumed to be uncorrelated among points with large separations in Q^2 .
3. All correlations for the same “theoretical source” are 100% except for the \mathcal{O}_6 one, which is assumed to be uncorrelated among points with large separations in Q^2 .
4. All correlations for the same “theoretical source” are 100% except for the scale uncertainties and the \mathcal{O}_6 ones, which are assumed to be uncorrelated among points with large separations in Q^2 .

7.3 Results

The numerical results obtained with the four different assumptions on the theoretical correlations are displayed in Tables 5, 6, 7 and 8, respectively. Each table shows the average values of $\alpha_s^{(n_f=5)}(M_Z^2)$ extracted from the four different choices of Q^2 points (sets 1, 2, 1* and 2*) and with the three different averaging procedures: χ^2 minimisation, simple average and weighted average. Clearly, the results in Table 5 have too large χ^2 values associated to them, both for sets 1 and 2. As explained above, this is not necessarily a signature of inconsistent experimental data sets, but can also be due to the limitations explained in Sec. 7.1. Much more reasonable values are obtained by taking points with broader separation in Q^2 , *i.e.* the set 1*, or with the alternative choices for the theoretical correlations proposed in Sec. 7.2.

²¹In Ref. [133] one can find further discussions on unbiased combination procedures. These feature realistic uncertainty estimates, based on the propagation of the full information on the uncertainties of the inputs, with their correlations.

	χ^2	Minimisation	χ^2	Simple Average	χ^2	Weighted Average
Set 1	11.2	0.1190(16)(7)(12)	18.6	0.1133(18)(12)(17)	18.8	0.1132(18)(12)(18)
Set 2	8.8	0.1198(8)(3)(13)	22.4	0.1139(19)(11)(12)	22.4	0.1140(19)(11)(12)
Set 1*	1.5	0.1149(19)(13)(8)	1.8	0.1133(18)(12)(18)	1.9	0.1132(19)(12)(19)
Set 2*	4.3	0.1163(19)(10)(7)	5.3	0.1139(19)(11)(12)	5.3	0.1140(19)(11)(12)

Table 5. Averaged results for $\alpha_s^{(n_f=5)}(M_Z^2)$ obtained when the theory uncertainties originating from the same source are assumed to be fully correlated.

	χ^2	Minimisation	χ^2	Simple Average	χ^2	Weighted Average
Set 1	1.9	0.1148(20)(11)(9)	2.2	0.1133(18)(12)(17)	2.3	0.1132(18)(12)(18)
Set 2	2.8	0.1155(19)(11)(10)	3.2	0.1139(19)(11)(12)	3.2	0.1140(19)(11)(12)
Set 1*	1.3	0.1147(20)(11)(9)	1.7	0.1133(18)(12)(19)	1.7	0.1132(19)(12)(19)
Set 2*	2.7	0.1155(19)(11)(9)	3.1	0.1139(19)(11)(12)	3.1	0.1140(19)(11)(12)

Table 6. Averaged results for $\alpha_s^{(n_f=5)}(M_Z^2)$ obtained when the theory uncertainties from scale variations are assumed to be uncorrelated.

All in all we find that there is not much gain in combining several Q^2 values. We observe that the minimisation procedure yields a bias towards larger values of α_s , which are preferred by the (potentially dangerous) directions associated to small eigenvalues of the original covariance matrix. Once these are treated more conservatively (*i.e.* Tables 6, 7 and 8), one suppresses the associated bias and obtains values much more compatible with the ones from the other averaging procedures. As expected, the associated α_s values cluster around

$$\alpha_s^{(n_f=5)}(M_Z^2) = 0.1136 \pm 0.0025, \quad (7.6)$$

which is approximately 2σ below the FLAG lattice average. The corresponding fit to lattice data (see App. C) returns larger values clustering around²²

$$\alpha_s^{(n_f=5)}(M_Z^2) = 0.1179 \pm 0.0025, \quad (7.7)$$

exhibiting again the discrepancy between the dispersive and the lattice-based results. Nevertheless, this also shows that, once the situation with respect to the different tensions related to $R(s)$ is clarified, a determination of $\alpha_s^{(n_f=5)}(M_Z^2)$ with a precision of $\mathcal{O}(1\%)$ could be achievable from the Euclidean Adler function.

In the combinations of pairs of $\alpha_s^{(n_f=5)}(M_Z^2)$ values evaluated at different Q^2 points, the derived χ^2 values also provide an implicit test of the RGE (used for evolving $\alpha_s^{(n_f=5)}$ from each Q^2 point to M_Z^2), within the assumptions for the treatment of the uncertainties and of their correlations discussed above. We implement an alternative approach of testing the RGE. It consists in computing the differences between the extracted $\alpha_s^{(n_f=5)}(M_Z^2)$ values

²²Note that the uncertainties in these two combinations (with a different hierarchy compared to Fig. 19) strongly depend on the estimated correlations between the combined points, see Figs. 12 and 14, which in the lattice case is based on Eqs. (4.1) and (4.2).

	χ^2	Minimisation	χ^2	Simple Average	χ^2	Weighted Average
Set 1	2.0	0.1148(20)(11)(9)	2.4	0.1133(18)(12)(16)	2.5	0.1132(18)(12)(17)
Set 2	3.9	0.1160(18)(10)(9)	4.7	0.1139(19)(11)(12)	4.7	0.1140(19)(11)(12)
Set 1*	1.2	0.1146(20)(11)(10)	1.4	0.1133(18)(12)(17)	1.5	0.1132(19)(12)(18)
Set 2*	2.9	0.1156(19)(11)(9)	3.3	0.1139(19)(11)(12)	3.3	0.1140(19)(11)(12)

Table 7. Averaged results for $\alpha_s^{(n_f=5)}(M_Z^2)$ obtained when the theory uncertainty from \mathcal{O}_6 is assumed to be uncorrelated.

	χ^2	Minimisation	χ^2	Simple Average	χ^2	Weighted Average
Set 1	1.6	0.1145(19)(11)(10)	1.8	0.1133(18)(12)(16)	1.9	0.1132(18)(12)(17)
Set 2	2.3	0.1152(19)(11)(10)	2.6	0.1139(19)(11)(11)	2.6	0.1140(19)(11)(11)
Set 1*	1.1	0.1145(19)(11)(10)	1.3	0.1133(18)(12)(17)	1.4	0.1132(19)(12)(18)
Set 2*	2.1	0.1151(19)(11)(10)	2.3	0.1139(19)(11)(12)	2.3	0.1140(19)(11)(12)

Table 8. Averaged results for $\alpha_s^{(n_f=5)}(M_Z^2)$ obtained when the theory uncertainties from scale variations and \mathcal{O}_6 are assumed to be uncorrelated.

at some reference Q^2 point (in this case 5.41 GeV^2 , yielding the most precise $\alpha_s^{(n_f=5)}(M_Z^2)$ value among the Q^2 points considered here) and each of the other considered Q^2 points respectively. We also compute the corresponding relative differences normalised with respect to the former (reference) $\alpha_s^{(n_f=5)}(M_Z^2)$ value (see Fig. 20). The uncertainties on these differences are evaluated through a linear error propagation, taking into account the full information on the correlations among the uncertainties of the two corresponding $\alpha_s^{(n_f=5)}(M_Z^2)$ input values. The significance of the deviation from zero for each of these differences, computed as the difference divided by its uncertainty, represents a test of the RGE within the Q^2 range of the two points that are being considered.²³ In addition, the uncertainty of each such difference provides a measure of the precision within which the RGE test has been performed. This represents an important information, in addition to the Q^2 range and to the outcome of the test itself. Indeed, we observe that the RGE test here is performed within a precision between 1.4 permil and about two percent, depending on the Q^2 range and the correlation assumptions employed for the theory uncertainties. This can be seen in the plots at the bottom of Fig. 20, where we display the differences between the extracted $\alpha_s^{(n_f=5)}(M_Z^2)$ value at $Q^2 = 5.41 \text{ GeV}^2$ and the rest of extracted values of Table 4, normalised by the former.²⁴

²³The significance squared for the simple differences corresponds to the minimum of the χ^2 in Eq. (7.3) (see e.g. Ref. [134]). Very similar values are obtained for the significance of the relative differences squared (up to small non-linear effects in the uncertainty propagation). We have also checked this correspondence numerically in the current study.

²⁴The analogous plots using instead lattice data are once again relegated to App. C.

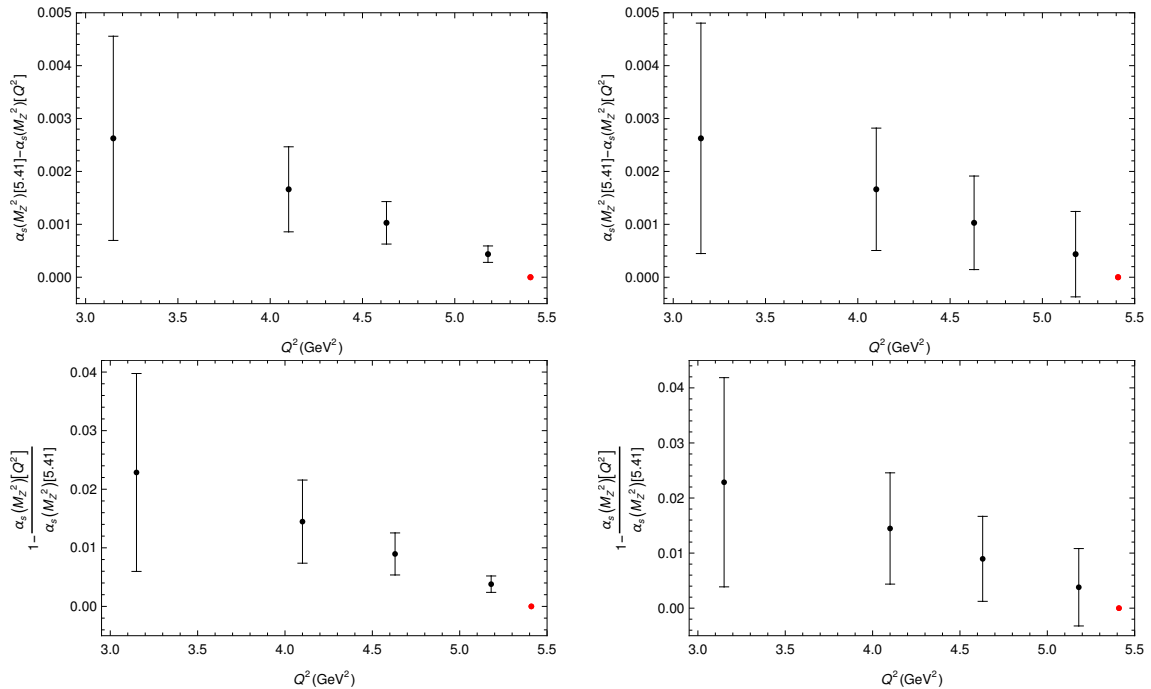


Figure 20. The top plots show the differences between the extracted $\alpha_s^{(n_f=5)}(M_Z^2)$ value at $Q^2 = 5.41$ GeV 2 and the rest of extracted values in Table 4, together with their uncertainties computed taking into account the correlations. The bottom plots show the same differences normalised with respect to the $\alpha_s^{(n_f=5)}(M_Z^2)$ value extracted at $Q^2 = 5.41$ GeV 2 . The red circle indicates the reference point at $Q^2 = 5.41$ GeV 2 . For the left plots we assume the theory uncertainties originating from the same source to be fully correlated, whereas for the right plots we assume the theory uncertainties from scale variations and \mathcal{O}_6 to be uncorrelated.

8 Conclusions

In this work we have carefully analysed the QCD predictions for the electromagnetic Euclidean Adler function, below the charm threshold. It was already known that this observable could be studied within pQCD from relatively low energies. From the phenomenological point of view, this is relevant because one can independently determine it at relatively low energies from recent precise e^+e^- and lattice data, which are known to produce results in clear tension with each other. A comparison between these three different determinations of the Adler function is then compelling because 1. pQCD may discriminate, up to a certain extent, between the e^+e^- -based and the latticed-based Adler functions if they do not agree. 2. Assuming the validity of one of them, one can test the validity domain of pQCD, just at the edge of the perturbative breakdown. 3. One can study the sensitivity to the QCD coupling of a direct comparison between pQCD and the ratio $R(s)$.

In order to unlock the full potential from known pQCD results at relatively low energies, a consistent analysis beyond the available $\mathcal{O}(\alpha_s^2)$ precision in mass-dependent (decoupling) schemes such as MOM was preferred. Most of this work has consisted in assembling all the needed pieces in an EFT-based $\overline{\text{MS}}$ set-up, to perform such a comparison at $\mathcal{O}(\alpha_s^4)$, with

a careful treatment of all associated expansions and uncertainties. This has been done in Sec. 3, where many details are given in order to simplify the reproducibility of our results and facilitate future applications and improvements. The extraction of alternative Adler functions, based on $R(s)$ data and lattice results, has been studied in Sec. 4.

We have first compared in Sec. 5 the pure perturbative predictions with the results obtained from both e^+e^- data and lattice QCD, confirming (although at a somewhat reduced level) the tension observed in $g-2$ between these two different approaches. Taking as input the value of α_s from the FLAG compilation, $\alpha_s^{(n_f=5)}(M_Z^2) = 0.1184 \pm 0.0008$, the pQCD prediction of the Adler function turns out to be in excellent agreement with the lattice determination at $Q^2 \gtrsim 2 \text{ GeV}^2$, while the determination from e^+e^- data lies systematically below it in the energy range $Q^2 \in [1, 5.5] \text{ GeV}^2$.

In Sec. 6 we have incorporated the leading nonperturbative power corrections, in order to have a better assessment of the theoretical uncertainties in the lowest range of Q^2 values. Once these corrections are taken into account, the agreement between the QCD OPE prediction and the lattice result extends to the whole analysed range of Q^2 , although the theoretical uncertainties turn out to be large below 2 GeV^2 .

Assuming the validity of the OPE at $Q \approx 2 \text{ GeV}$, the Adler function extracted from the e^+e^- data lies approximately 2σ below the OPE predictions. This appears to follow the same trend as the deficit observed in the muon $g-2$ integral, when comparing the dispersive e^+e^- estimate to both the experimental measurement of the muon anomalous magnetic moment and the lattice results, as well as the deficit observed by different lattice groups for the window integral and the deficit in the hadronic running of α when compared to the lattice result from Ref. [14].

In order to fit the Adler function extracted from e^+e^- data, one would need values of the strong coupling significantly below the current lattice (and PDG) average and/or much larger nonperturbative corrections that would not scale with the expected power corrections. Both possibilities are disfavoured by the lattice data that match beautifully the pQCD predictions, at the achieved precision, even at energies as low as $Q \sim 1.25 \text{ GeV}$.

On the other hand, several possible applications can be expected from our study. Combining the results of this work with future lattice studies could help in assessing the validity domain of pQCD for the different involved correlators at higher precision, while at large Q^2 values, where pQCD is more reliable, the corresponding results can help in understanding discretization effects in the lattice. We also leave for future work exploring an alternative implementation of the Euclidean running of α , based on EFTs (using the $\overline{\text{MS}}$ scheme) supplemented by appropriate energy expansions and possibly interpolations, just starting from the massless descriptions at the different number of flavors, as we have done in this first work at $n_f = 3$. This can also be combined with lattice data, as shown in [14, 39].

Once the current tensions between the lattice QCD and data-driven approaches (which are also very relevant in the context of the anomalous magnetic moment of the muon) are resolved, the comparison between data and QCD could provide a determination of $\alpha_s^{(n_f=5)}(M_Z^2)$ at the per-cent level. With this respect, forthcoming precise measurements

of the hadronic production cross-sections, as well as independent lattice calculations of similar precision, will play a major role.

Acknowledgements

MD, BM and ZZ would like to acknowledge their fruitful collaboration with Andreas Hoecker. We are also grateful to Andrei Kataev, Eduardo de Rafael and Harmut Wittig for useful comments on the manuscript ARS was supported by European Union’s Horizon 2020 research and innovation programme under grant agreement No 101002846, ERC CoG “CosmoChart” and funded in part by MIUR contract number 2017L5W2PT. ARS and BM acknowledge the support from LPNHE, CNRS/IN2P3, Sorbonne Université. BM is also supported by Université de Paris. DDC and AP are supported in part by Generalitat Valenciana, Grant No. Prometeo/2021/071, and MCIN/AEI/10.13039/501100011033, Grant No. PID2020-114473GB-I00. DDC was funded in part by CIDEAGENT/2018/014.

A Compilation of perturbative coefficients

In this section we compile the different coefficients used to evaluate the perturbative Adler function, in the $\overline{\text{MS}}$ renormalization scheme.

A.1 Running of α_s , quark masses and decoupling relations

The known β -function coefficients associated with the running of α_s ,

$$\mu \frac{d\alpha_s}{d\mu} = \alpha_s \beta(\alpha_s), \quad \beta(\alpha_s) = \sum_{n=1} \beta_n \left(\frac{\alpha_s}{\pi} \right)^n, \quad (\text{A.1})$$

are [135–143]

$$\beta_1 = \frac{1}{3} n_f - \frac{11}{2}, \quad \beta_2 = -\frac{51}{4} + \frac{19}{12} n_f, \quad (\text{A.2})$$

$$\beta_3 = \frac{1}{64} \left[-2857 + \frac{5033}{9} n_f - \frac{325}{27} n_f^2 \right], \quad (\text{A.3})$$

$$\beta_4 = \frac{-1}{128} \left[\frac{149753}{6} + 3564 \zeta_3 - \left(\frac{1078361}{162} + \frac{6508}{27} \zeta_3 \right) n_f + \left(\frac{50065}{162} + \frac{6472}{81} \zeta_3 \right) n_f^2 + \frac{1093}{729} n_f^3 \right], \quad (\text{A.4})$$

$$\begin{aligned} \beta_5 = -\frac{1}{512} & \left\{ \frac{8157455}{16} + \frac{621885}{2} \zeta_3 - \frac{88209}{2} \zeta_4 - 288090 \zeta_5 \right. \\ & + n_f \left[-\frac{336460813}{1944} - \frac{4811164}{81} \zeta_3 + \frac{33935}{6} \zeta_4 + \frac{1358995}{27} \zeta_5 \right] \\ & + n_f^2 \left[\frac{25960913}{1944} + \frac{698531}{81} \zeta_3 - \frac{10526}{9} \zeta_4 - \frac{381760}{81} \zeta_5 \right] \\ & \left. + n_f^3 \left[-\frac{630559}{5832} - \frac{48722}{243} \zeta_3 + \frac{1618}{27} \zeta_4 + \frac{460}{9} \zeta_5 \right] + n_f^4 \left[\frac{1205}{2916} - \frac{152}{81} \zeta_3 \right] \right\}. \quad (\text{A.5}) \end{aligned}$$

The RGE for the running masses is

$$\mu \frac{dm_q}{d\mu} = -m_q \gamma(\alpha_s), \quad \gamma(\alpha_s) = \sum_{n=1} \gamma_n \left(\frac{\alpha_s}{\pi} \right)^n. \quad (\text{A.6})$$

The known coefficients are [144–150]

$$\gamma_1 = 2, \quad \gamma_2 = \frac{101}{12} - \frac{5}{18} n_f, \quad (\text{A.7})$$

$$\gamma_3 = \frac{1}{24} \left[\frac{3747}{4} - \left(\frac{554}{9} + 40 \zeta_3 \right) n_f - \frac{35}{27} n_f^2 \right], \quad (\text{A.8})$$

$$\begin{aligned} \gamma_4 = \frac{1}{128} \left\{ \frac{4603055}{162} + \frac{135680}{27} \zeta_3 - 8800 \zeta_5 + n_f \left[-\frac{91723}{27} - \frac{34192}{9} \zeta_3 + 880 \zeta_4 + \frac{18400}{9} \zeta_5 \right] \right. \\ \left. + n_f^2 \left[\frac{5242}{243} + \frac{800}{9} \zeta_3 - \frac{160}{3} \zeta_4 \right] + n_f^3 \left[-\frac{332}{243} + \frac{64}{27} \zeta_3 \right] \right\}, \quad (\text{A.9}) \end{aligned}$$

$$\begin{aligned} \gamma_5 = \frac{1}{512} \left\{ \frac{99512327}{162} + \frac{46402466}{243} \zeta_3 + 96800 \zeta_3^2 - \frac{698126}{9} \zeta_4 - \frac{231757160}{243} \zeta_5 + 242000 \zeta_6 + 412720 \zeta_7 \right. \\ \left. + n_f \left[-\frac{150736283}{1458} - \frac{12538016}{81} \zeta_3 - \frac{75680}{9} \zeta_3^2 + \frac{2038742}{27} \zeta_4 + \frac{49876180}{243} \zeta_5 - \frac{638000}{9} \zeta_6 \right. \right. \\ \left. \left. - \frac{1820000}{27} \zeta_7 \right] \right. \\ \left. + n_f^2 \left[\frac{1320742}{729} + \frac{2010824}{243} \zeta_3 + \frac{46400}{27} \zeta_3^2 - \frac{166300}{27} \zeta_4 - \frac{264040}{81} \zeta_5 + \frac{92000}{27} \zeta_6 \right] \right. \\ \left. + n_f^3 \left[\frac{91865}{1458} + \frac{12848}{81} \zeta_3 + \frac{448}{9} \zeta_4 - \frac{5120}{27} \zeta_5 \right] + n_f^4 \left[-\frac{260}{243} - \frac{320}{243} \zeta_3 + \frac{64}{27} \zeta_4 \right] \right\}. \quad (\text{A.10}) \end{aligned}$$

A.2 Light-quark loop coefficients

In the limit of n_f massless quarks and no extra (or infinitely massive) heavy quarks the Adler function is determined by the $K_{n,0}$, coefficients²⁵

$$D_{ii}^{L,(0)}(Q^2) = N_C \left\{ 1 + \sum_{n=1} K_{n,0} \left(\frac{\alpha_s(Q^2)}{\pi} \right)^n \right\}. \quad (\text{A.11})$$

They are [56, 151–159]

$$\begin{aligned} K_{1,0} &= 1, & K_{2,0} &= \frac{365}{24} - 11 \zeta_3 + \left(\frac{2}{3} \zeta_3 - \frac{11}{12} \right) n_f, \\ K_{3,0} &= \frac{87029}{288} - \frac{1103}{4} \zeta_3 + \frac{275}{6} \zeta_5 + \left(-\frac{7847}{216} + \frac{262}{9} \zeta_3 - \frac{25}{9} \zeta_5 \right) n_f + \left(\frac{151}{162} - \frac{19}{27} \zeta_3 \right) n_f^2, \\ K_{4,0} &= \frac{144939499}{20736} - \frac{5693495}{864} \zeta_3 + \frac{5445}{8} \zeta_3^2 + \frac{65945}{288} \zeta_5 - \frac{7315}{48} \zeta_7 \end{aligned}$$

²⁵Again we do not display here the singlet contributions (see main text).

$$\begin{aligned}
& + \left(-\frac{13044007}{10368} + \frac{12205}{12} \zeta_3 - 55 \zeta_3^2 + \frac{29675}{432} \zeta_5 + \frac{665}{72} \zeta_7 \right) n_f \\
& + \left(\frac{1045381}{15552} - \frac{40655}{864} \zeta_3 + \frac{5}{6} \zeta_3^2 - \frac{260}{27} \zeta_5 \right) n_f^2 + \left(-\frac{6131}{5832} + \frac{203}{324} \zeta_3 + \frac{5}{18} \zeta_5 \right) n_f^3.
\end{aligned} \tag{A.12}$$

Following the notation of Ref. [36], the strange mass corrections are given by a linear combination of three coefficients

$$\Delta_{m_s} D_{33}^L(Q^2) = -3N_C \frac{m_s^2(Q)}{Q^2} \sum_n (2c_n^{L+T} + e_n^{L+T} + f_n^{L+T}) \left(\frac{\alpha_s(Q^2)}{\pi} \right)^n + \mathcal{O} \left(\frac{m_s^4}{Q^4} \right) \tag{A.13}$$

In general they are all known up to three loops [160–163],

$$c_0^{L+T} = 1, \quad c_1^{L+T} = \frac{13}{3}, \quad c_2^{L+T} = \frac{25291}{432} + \frac{215}{54} \zeta_3 - \frac{520}{27} \zeta_5 - n_f \left(\frac{41}{24} + \frac{2}{9} \zeta_3 \right), \tag{A.14}$$

$$e_0^{L+T} = 0, \quad e_1^{L+T} = \frac{2}{3}, \quad e_2^{L+T} = \frac{877}{54} - \frac{91}{27} \zeta_3 - \frac{5}{27} \zeta_5 - n_f \left(\frac{2}{3} - \frac{4}{9} \zeta_3 \right), \tag{A.15}$$

$$f_0^{L+T} = 0, \quad f_1^{L+T} = 0, \quad f_2^{L+T} = -\frac{32}{9} + \frac{8}{3} \zeta_3, \tag{A.16}$$

but in fact the needed linear combination is known up to four loops [164]

$$\begin{aligned}
2c_3^{L+T} + e_3^{L+T} + f_3^{L+T} &= \frac{16828967}{7776} - \frac{12295}{81} \zeta_3 + \frac{7225}{108} \zeta_3^2 - \frac{93860}{81} \zeta_5 + \frac{1027019}{2592} \zeta_7 \\
&- n_f \left(\frac{33887}{216} + \frac{721}{486} \zeta_3 + \frac{106}{27} \zeta_3^2 + \frac{5}{3} \zeta_4 - \frac{10355}{243} \zeta_5 \right) \\
&+ n_f^2 \left(\frac{9661}{5832} + \frac{2}{27} \zeta_3 \right).
\end{aligned} \tag{A.17}$$

A.3 Heavy-quark loop coefficients

The contribution to the Adler function from heavy-quark loops depends on the $\bar{C}_j^{(n)}(\mu)$ coefficients defined in Eqs. (3.17) and (3.18). In Table 9 we compile the known (non-singlet) coefficients $\bar{C}_j^{(n)}(m_c(m_c))$, up to $j = 10$ and $n = 3$, taken from the references referred in the main text. Let us remark that for $n = 3, j > 4$ they are only approximated values. The $n = 3$ singlet contribution is given separately in Eq. (3.21).

Using the scale-invariance of the Adler function and the RGE of the running coupling and masses, it is straightforward to find the values of these coefficients at any other renormalization scale. For example, for the four-loop coefficients one finds:

$$\begin{aligned}
\bar{C}_1^{(3)}(\mu) &= \bar{C}_1^{(3)}(m_c(m_c)) + \frac{26}{405} L^3 - \frac{42001}{10935} L^2 + \left(-\frac{21640907}{233280} \zeta(3) + \frac{144646921}{1049760} \right) L, \\
\bar{C}_2^{(3)}(\mu) &= \bar{C}_2^{(3)}(m_c(m_c)) - \frac{92}{945} L^3 + \frac{1236401}{127575} L^2 + \left(-\frac{160906453}{3483648} \zeta(3) + \frac{1514929311547}{17635968000} \right) L, \\
\bar{C}_3^{(3)}(\mu) &= \bar{C}_3^{(3)}(m_c(m_c)) + \frac{16544}{8505} L^3 + \frac{301549372}{13395375} L^2 + \left(\frac{588425644445059}{240045120000} \zeta_3 - \frac{2101159030799659}{720135360000} \right) L,
\end{aligned}$$

j	$\bar{C}_j^{(0)}(m_c(m_c))$	$\bar{C}_j^{(1)}(m_c(m_c))$	$\bar{C}_j^{(2)}(m_c(m_c))$	$\bar{C}_j^{(3)}(m_c(m_c))$
1	1.0667	2.5547	2.4967	-5.6404
2	0.4571	1.1096	2.7770	-3.4937
3	0.2709	0.5194	1.6389	-2.8395
4	0.1847	0.2031	0.7956	-3.349
5	0.1364	0.0106	0.2781	-3.737
6	0.1061	-0.1158	0.0070	-3.735
7	0.0856	-0.2033	-0.0859	-3.39
8	0.0709	-0.2660	-0.0496	-2.85
9	0.0601	-0.3122	0.0817	-2.22
10	0.0517	-0.3470	0.2838	-1.65

Table 9. Non-singlet heavy-quark coefficients $\bar{C}_j^{(n)}(m_c(m_c))$. The values given for $\bar{C}_{j>4}^{(3)}(m_c(m_c))$ are only approximate estimates.

$$\bar{C}_4^{(3)}(\mu) = \bar{C}_4^{(3)}(m_c(m_c)) \frac{104512}{18711} L^3 + \frac{1207474918}{37889775} L^2 + \left(\frac{3882485996940952}{139244923125} \zeta_3 - \frac{4663762048907267}{139244923125} \right) L,$$

$$\bar{C}_5^{(3)}(\mu) = \bar{C}_5^{(3)}(m_c(m_c)) + \frac{121600}{11583} L^3 + \frac{419559137}{11188131} L^2 + \left(\frac{11493749549904284922937344}{51676194450456575903} \zeta_3 - \frac{13815337731941240844320768}{51676194450456575903} \right) L,$$

$$\bar{C}_6^{(3)}(\mu) = \bar{C}_6^{(3)}(m_c(m_c)) + \frac{2863616}{173745} L^3 + \frac{917112400}{23175603} L^2 + \left(\frac{651547528689568126172154298368}{429356162878789378794041} \zeta_3 - \frac{783193764656552535030069460992}{429356162878789378794041} \right) L,$$

$$\bar{C}_7^{(3)}(\mu) = \bar{C}_7^{(3)}(m_c(m_c)) + \frac{483328}{20655} L^3 + \frac{584955462}{15264583} L^2 + \left(\frac{535501006096859255438313967560163328}{56757449883272928029520032067} \zeta_3 - \frac{1931107816850828622369214941259366400}{170272349649818784088560096201} \right) L,$$

$$\begin{aligned} \bar{C}_8^{(3)}(\mu) &= \bar{C}_8^{(3)}(m_c(m_c)) + \frac{194265088}{6235515} L^3 + \frac{488784115}{14385877} L^2 \\ &+ \left(\frac{3604714064840321574346924622791084364267520}{65447583034900845993238160708606879} \zeta_3 - \frac{4333071686738680398413127461273056938295296}{65447583034900845993238160708606879} \right) L, \end{aligned}$$

$$\bar{C}_9^{(3)}(\mu) = \bar{C}_9^{(3)}(m_c(m_c)) + \frac{1038942208}{26189163} L^3 + \frac{499493070}{18676903} L^2$$

$$\begin{aligned}
& + \left(\frac{159592894419467095119221552398948945854700978176}{519784704463182451617731521986046572497} \zeta_3 \right. \\
& \left. - \frac{191839744405509297915091679432644835963148697600}{519784704463182451617731521986046572497} \right) L, \\
\bar{C}_{10}^{(3)}(\mu) &= \bar{C}_{10}^{(3)}(m_c(m_c)) + \frac{140902400}{2882061} L^3 + \frac{178198601}{10606396} L^2 \\
& + \left(\frac{21882965916951934885062063776238518244057546752}{13246590806263931598330852967289655819} \zeta_3 \right. \\
& \left. - \frac{26304570367320737503829762957552484175252029440}{13246590806263931598330852967289655819} \right) L,
\end{aligned}$$

where $L \equiv \log\left(\frac{m_c^2(m_c)}{\mu^2}\right)$.

B Interplay of $\bar{\Pi}^{08}$ with perturbative QCD

In Ref. [14], the rational approximation of another correlator, obtained using lattice data, is presented, Π^{08} , which is defined as,

$$\bar{\Pi}^{08}(Q^2) \equiv \frac{1}{4\sqrt{3}} \sum_{i,j} Q_8^i \bar{\Pi}_{ij}(Q^2), \quad \vec{Q}_8 \equiv \{1, 1, -2\}. \quad (\text{B.1})$$

Let us check what can we learn using analytic methods. First, it can be rewritten as

$$\bar{\Pi}^{08}(Q^2) = \frac{1}{4\sqrt{3}} \left(2(\bar{\Pi}_{ll} - \bar{\Pi}_{33}) + \sum_{i,j \neq i} Q_8^i \bar{\Pi}_{ij} \right). \quad (\text{B.2})$$

We have defined

$$\bar{\Pi}_{ll} \equiv \frac{\bar{\Pi}_{11} + \bar{\Pi}_{22}}{2}. \quad (\text{B.3})$$

From Eq. (B.2) it is straightforward to see that the correlator vanishes at all orders in massless perturbative QCD, since in that limit $\bar{\Pi}_{ll} = \bar{\Pi}_{33}$ and the disconnected topology associated to the second term, which in general starts at $\mathcal{O}(\alpha_s^3)$, vanishes for the sum.

The leading OPE contribution to $\bar{\Pi}^{08}(Q^2)$ is then given by the perturbative mass correction, scaling as $\sim \frac{m_s^2}{Q^2}$, so that $\bar{\Pi}^{08}(Q^2 \rightarrow \infty) = \Pi^{08}(Q^2 \rightarrow 0)$. In fact, let us note that this asymptotic scaling implies that the correlator satisfies an unsubtracted dispersion relation,

$$\Pi^{08}(Q^2) = \frac{1}{\pi} \int_{|Q_{\text{th}}|^2}^{\infty} dQ'^2 \frac{\text{Im}\Pi^{08}(Q'^2 e^{-i\pi})}{Q'^2 + Q^2}. \quad (\text{B.4})$$

The associated (massive) perturbative Adler function is, safely neglecting $m_{u,d}$, simply given by

$$D^{08}(Q^2) = -\frac{1}{2\sqrt{3}} \{ \Delta_{m_s} D_{33}^L(Q^2) + \Delta_{m_s} D_{3l}(Q^2) \}, \quad (\text{B.5})$$

where $\Delta_{m_s} D_{33}^L(Q^2)$ and $\Delta_{m_s} D_{3l}(Q^2)$ refer to the strange mass correction of the associated correlators, being $\Delta_{m_s} D_{3l}(Q^2) = \frac{1}{2} [\Delta_{m_s} D_{3u}(Q^2) + \Delta_{m_s} D_{3d}(Q^2)]$. Within the large perturbative uncertainties, the second term, which only starts at $\mathcal{O}(\alpha_s^3)$ and comes with an

extra $\mathcal{O}\left(\frac{1}{N_c}\right)$ suppression, can be safely neglected. We can then recall Eq. (3.9) to arrive at the perturbative result, valid at large Q^2 :²⁶

$$D_{\text{pQCD}}^{08}(Q^2) = \frac{\sqrt{3}}{2} N_C \frac{m_s^2(Q^2)}{Q^2} \sum_n (2c_n^{L+T} + e_n^{L+T} + f_n^{L+T}) \left(\frac{\alpha_s(Q^2)}{\pi}\right)^n. \quad (\text{B.6})$$

Since the perturbative QCD contributions are suppressed by two powers of the energy, one may expect nonperturbative effects to be numerically more relevant. They only enter suppressed by two extra powers of the energy and, additionally, they are linear instead of quadratic in the small strange quark mass, since the chirality-conserving nature of the vector current insertions can be recovered by combining a chirality-flipping insertion of the strange quark mass with a second one from the quark condensate. The associated contribution is

$$D^{08}(Q^2) = -\frac{24\pi^2}{\sqrt{3}Q^4} m_s \langle \bar{s}s \rangle \left(1 + \frac{\alpha_s}{3\pi}\right). \quad (\text{B.7})$$

Let us then take the corresponding rational approximation given in Ref. [14],

$$\bar{\Pi}^{08}(Q^2) = \frac{0.0217(11)x + 0.0151(12)x^2}{1 + 2.93(8)x + 2.15(12)x^2}, \quad x = \frac{Q^2}{\text{GeV}^2}, \quad (\text{B.8})$$

where the numerator a_i and denominator b_j parameters are strongly correlated according to

$$\text{corr} \begin{pmatrix} a_1 \\ a_2 \\ b_1 \\ b_2 \end{pmatrix} = \begin{pmatrix} 1 & & & \\ 0.97 & 1 & & \\ 0.97 & 0.984 & 1 & \\ 0.944 & 0.994 & 0.98 & 1 \end{pmatrix}, \quad (\text{B.9})$$

and compare it to the perturbative and OPE descriptions. The result is displayed in Fig. 21. In spite of the extremely bad behaviour of the associated pQCD series, which fortunately plays a very marginal quantitative role in the EM Adler function, an excellent agreement to pQCD (with a somewhat arbitrary truncation criteria) appears to emerge up to $Q^2 \sim 5 \text{ GeV}^2$. However, when incorporating the $D = 4$ power correction, a slight tension emerges. Given the different scaling both in energy and in strange quark mass of the pQCD series, $\sim \frac{m_s^2}{Q^2}$, with respect to the leading power corrections $\sim \frac{m_s \Lambda_{\text{QCD}}^3}{Q^4}$ and with respect to higher power corrections, most likely dominated by a quark-gluon condensate scaling as $\sim \frac{m_s \Lambda_{\text{QCD}}^5}{Q^6}$, comparisons to further lattice simulations at different strange quark masses and at different (relatively large) Q^2 values could shed some further light on where the rigorous OPE limits are fulfilled for the corresponding correlator.

C Fit results for α_s using lattice data

For completeness we provide in this appendix the corresponding lattice data results for Tables 4-8 in Tables 10-14. The lattice version of Fig. 20 is shown in Fig. 22.

²⁶Once again, the very poor behaviour of this perturbative series at small Q^2 can be seen in Table 2.

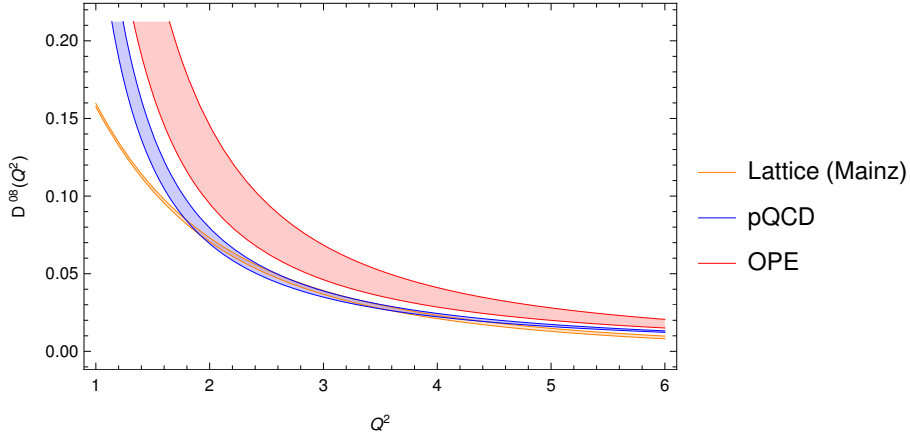


Figure 21. Comparison between the Adler function $D^{08}(Q^2)$ obtained from the lattice results of Ref. [14] and the one from the OPE of the associated correlator.

	Q^2	$\alpha_s(M_Z^2)$
Set 1	3.15	0.1177(40) _{Latt} (19) _{th}
	4.10	0.1174(31) _{Latt} (13) _{th}
	5.18	0.1181(22) _{Latt} (10) _{th}
Set 2	4.10	0.1174(31) _{Latt} (13) _{th}
	4.63	0.1176(23) _{Latt} (11) _{th}
	5.41	0.1185(24) _{Latt} (9) _{th}

Table 10. The two sets of three Q^2 points chosen for the averages with their uncertainties using lattice data.

	χ^2	Minimisation	χ^2	Simple Average	χ^2	Weighted Average
Set 1	1.1	0.1185(23)	1.2	0.1178(30)	1.1	0.1178(26)
Set 2	4.5	0.1205(21)	6.4	0.1178(25)	6.3	0.1179(24)
Set 1*	0.01	0.1181(24)	0.01	0.1179(28)	0.01	0.1180(24)
Set 2*	0.1	0.1182(23)	0.1	0.1179(24)	0.1	0.1181(24)

Table 11. Averaged results for $\alpha_s^{(n_f=5)}(M_Z^2)$ obtained when the theory uncertainties coming from the same source are assumed to be fully correlated.

	χ^2	Minimisation	χ^2	Simple Average	χ^2	Weighted Average
Set 1	0.4	0.1181(23)	0.4	0.1178(30)	0.4	0.1178(25)
Set 2	0.3	0.1182(23)	0.4	0.1178(24)	0.3	0.1179(24)
Set 1*	0.01	0.1181(24)	0.01	0.1179(28)	0.01	0.1180(24)
Set 2*	0.1	0.1182(23)	0.1	0.1179(24)	0.1	0.1181(23)

Table 12. Averaged results for $\alpha_s^{(n_f=5)}(M_Z^2)$ obtained when the theory uncertainties from scale variations are assumed to be uncorrelated.

	χ^2	Minimisation	χ^2	Simple Average	χ^2	Weighted Average
Set 1	0.3	0.1182(24)	0.4	0.1178(30)	0.4	0.1178(26)
Set 2	0.7	0.1184(23)	0.8	0.1178(25)	0.8	0.1179(24)
Set 1*	0.01	0.1181(24)	0.01	0.1179(28)	0.01	0.1180(24)
Set 2*	0.1	0.1182(23)	0.1	0.1179(24)	0.1	0.1181(23)

Table 13. Averaged results for $\alpha_s^{(n_f=5)}(M_Z^2)$ obtained when the theory uncertainty from \mathcal{O}_6 is assumed to be uncorrelated.

	χ^2	Minimisation	χ^2	Simple Average	χ^2	Weighted Average
Set 1	0.2	0.1181(23)	0.2	0.1178(29)	0.2	0.1178(25)
Set 2	0.3	0.1181(24)	0.3	0.1178(24)	0.3	0.1179(24)
Set 1*	0.01	0.1181(23)	0.01	0.1179(28)	0.01	0.1180(24)
Set 2*	0.1	0.1182(23)	0.1	0.1179(24)	0.1	0.1181(23)

Table 14. Averaged results for $\alpha_s^{(n_f=5)}(M_Z^2)$ obtained when the theory uncertainties from scale variations and \mathcal{O}_6 are assumed to be uncorrelated.

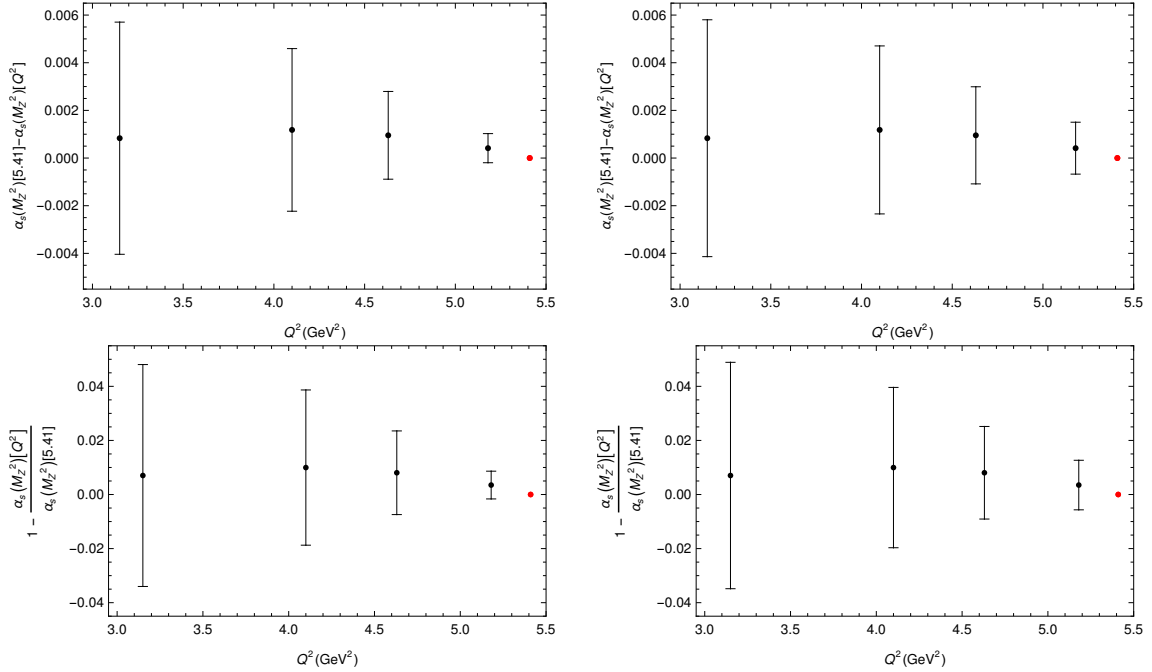


Figure 22. The same as Fig. 20 but using the results of Table 10.

D Full correlation matrices for the extracted $\alpha_s^{(n_f=5)}(M_Z^2)$ values

Full correlation matrix when the theory uncertainties coming from the same source are assumed to be fully correlated, Set 1:

$$\begin{pmatrix} 1. & & \\ 0.942 & 1. & \\ 0.838 & 0.971 & 1. \end{pmatrix}. \quad (\text{D.1})$$

Full correlation matrix when the theory uncertainties coming from the same source are assumed to be fully correlated, Set 2:

$$\begin{pmatrix} 1. & & \\ 0.986 & 1. & \\ 0.951 & 0.988 & 1. \end{pmatrix}. \quad (\text{D.2})$$

Full correlation matrix when the theory uncertainties from scale variations and \mathcal{O}_6 are assumed to be uncorrelated, Set 1:

$$\begin{pmatrix} 1. & & \\ 0.829 & 1. & \\ 0.768 & 0.917 & 1. \end{pmatrix}. \quad (\text{D.3})$$

Full correlation matrix when the theory uncertainties from scale variations and \mathcal{O}_6 are assumed to be uncorrelated, Set 2:

$$\begin{pmatrix} 1. & & \\ 0.912 & 1. & \\ 0.884 & 0.925 & 1. \end{pmatrix}. \quad (\text{D.4})$$

Full correlation matrix when the theory uncertainties from \mathcal{O}_6 are assumed to be uncorrelated, Set 1:

$$\begin{pmatrix} 1. & & \\ 0.829 & 1. & \\ 0.762 & 0.930 & 1. \end{pmatrix}. \quad (\text{D.5})$$

Full correlation matrix when the theory uncertainties from \mathcal{O}_6 are assumed to be uncorrelated, Set 2:

$$\begin{pmatrix} 1. & & \\ 0.941 & 1. & \\ 0.921 & 0.968 & 1. \end{pmatrix}. \quad (\text{D.6})$$

Full correlation matrix when the theory uncertainties from scale variations are assumed to be uncorrelated, Set 1:

$$\begin{pmatrix} 1. & & \\ 0.943 & 1. & \\ 0.882 & 0.940 & 1. \end{pmatrix}. \quad (\text{D.7})$$

Full correlation matrix when the theory uncertainties from scale variations are assumed to be uncorrelated, Set 2:

$$\begin{pmatrix} 1. & & \\ 0.956 & 1. & \\ 0.914 & 0.945 & 1. \end{pmatrix}. \quad (\text{D.8})$$

References

- [1] K.G. Wilson, *Nonlagrangian models of current algebra*, *Phys. Rev.* **179** (1969) 1499.
- [2] M.A. Shifman, A.I. Vainshtein and V.I. Zakharov, *QCD and Resonance Physics. Theoretical Foundations*, *Nucl. Phys. B* **147** (1979) 385.
- [3] M.A. Shifman, A.I. Vainshtein and V.I. Zakharov, *QCD and Resonance Physics: Applications*, *Nucl. Phys. B* **147** (1979) 448.
- [4] S.L. Adler, *Some Simple Vacuum Polarization Phenomenology: $e^+e^- \rightarrow$ Hadrons: The μ - Mesic Atom x -Ray Discrepancy and $g_\mu - 2$* , *Phys. Rev. D* **10** (1974) 3714.
- [5] J. Gasser and H. Leutwyler, *Chiral Perturbation Theory to One Loop*, *Annals Phys.* **158** (1984) 142.
- [6] J. Gasser and H. Leutwyler, *Chiral Perturbation Theory: Expansions in the Mass of the Strange Quark*, *Nucl. Phys. B* **250** (1985) 465.
- [7] G. Amoros, J. Bijnens and P. Talavera, *Two point functions at two loops in three flavor chiral perturbation theory*, *Nucl. Phys. B* **568** (2000) 319 [[hep-ph/9907264](#)].
- [8] V.A. Novikov, L.B. Okun, M.A. Shifman, A.I. Vainshtein, M.B. Voloshin and V.I. Zakharov, *Charmonium and Gluons: Basic Experimental Facts and Theoretical Introduction*, *Phys. Rept.* **41** (1978) 1.
- [9] A.I. Vainshtein, V.I. Zakharov and M.A. Shifman, *GLUON CONDENSATE AND LEPTON DECAYS OF VECTOR MESONS. (IN RUSSIAN)*, *JETP Lett.* **27** (1978) 55.
- [10] K. Chetyrkin, J.H. Kuhn, A. Maier, P. Maierhofer, P. Marquard, M. Steinhauser et al., *Precise Charm- and Bottom-Quark Masses: Theoretical and Experimental Uncertainties*, *Theor. Math. Phys.* **170** (2012) 217 [[1010.6157](#)].
- [11] K.G. Chetyrkin, J.H. Kuhn, A. Maier, P. Maierhofer, P. Marquard, M. Steinhauser et al., *Addendum to “Charm and bottom quark masses: An update”*, [1710.04249](#).
- [12] K.G. Wilson, *Confinement of Quarks*, *Phys. Rev. D* **10** (1974) 2445.
- [13] S. Borsanyi et al., *Leading hadronic contribution to the muon magnetic moment from lattice QCD*, *Nature* **593** (2021) 51 [[2002.12347](#)].
- [14] M. Cè, A. Gérardin, G. von Hippel, H.B. Meyer, K. Miura, K. Ottnad et al., *The hadronic running of the electromagnetic coupling and the electroweak mixing angle from lattice QCD*, *JHEP* **08** (2022) 220 [[2203.08676](#)].
- [15] FERMILAB LATTICE, LATTICE-HPQCD, MILC collaboration, *Strong-Isospin-Breaking Correction to the Muon Anomalous Magnetic Moment from Lattice QCD at the Physical Point*, *Phys. Rev. Lett.* **120** (2018) 152001 [[1710.11212](#)].

- [16] BUDAPEST-MARSEILLE-WUPPERTAL collaboration, *Hadronic vacuum polarization contribution to the anomalous magnetic moments of leptons from first principles*, *Phys. Rev. Lett.* **121** (2018) 022002 [[1711.04980](#)].
- [17] RBC, UKQCD collaboration, *Calculation of the hadronic vacuum polarization contribution to the muon anomalous magnetic moment*, *Phys. Rev. Lett.* **121** (2018) 022003 [[1801.07224](#)].
- [18] D. Giusti, V. Lubicz, G. Martinelli, F. Sanfilippo and S. Simula, *Electromagnetic and strong isospin-breaking corrections to the muon $g - 2$ from Lattice QCD+QED*, *Phys. Rev. D* **99** (2019) 114502 [[1901.10462](#)].
- [19] PACS collaboration, *Hadronic vacuum polarization contribution to the muon $g - 2$ with 2+1 flavor lattice QCD on a larger than $(10 \text{ fm})^4$ lattice at the physical point*, *Phys. Rev. D* **100** (2019) 034517 [[1902.00885](#)].
- [20] FERMILAB LATTICE, LATTICE-HPQCD, MILC collaboration, *Hadronic-vacuum-polarization contribution to the muon's anomalous magnetic moment from four-flavor lattice QCD*, *Phys. Rev. D* **101** (2020) 034512 [[1902.04223](#)].
- [21] A. Gérardin, M. Cè, G. von Hippel, B. Hörz, H.B. Meyer, D. Mohler et al., *The leading hadronic contribution to $(g - 2)_\mu$ from lattice QCD with $N_f = 2 + 1$ flavours of $O(a)$ improved Wilson quarks*, *Phys. Rev. D* **100** (2019) 014510 [[1904.03120](#)].
- [22] C. Aubin, T. Blum, C. Tu, M. Golterman, C. Jung and S. Peris, *Light quark vacuum polarization at the physical point and contribution to the muon $g - 2$* , *Phys. Rev. D* **101** (2020) 014503 [[1905.09307](#)].
- [23] D. Giusti and S. Simula, *Lepton anomalous magnetic moments in Lattice QCD+QED*, *PoS LATTICE2019* (2019) 104 [[1910.03874](#)].
- [24] M. Davier, A. Hoecker, B. Malaescu and Z. Zhang, *Reevaluation of the hadronic vacuum polarisation contributions to the Standard Model predictions of the muon $g - 2$ and $\alpha(m_Z^2)$ using newest hadronic cross-section data*, *Eur. Phys. J. C* **77** (2017) 827 [[1706.09436](#)].
- [25] A. Keshavarzi, D. Nomura and T. Teubner, *Muon $g - 2$ and $\alpha(M_Z^2)$: a new data-based analysis*, *Phys. Rev. D* **97** (2018) 114025 [[1802.02995](#)].
- [26] G. Colangelo, M. Hoferichter and P. Stoffer, *Two-pion contribution to hadronic vacuum polarization*, *JHEP* **02** (2019) 006 [[1810.00007](#)].
- [27] M. Hoferichter, B.-L. Hoid and B. Kubis, *Three-pion contribution to hadronic vacuum polarization*, *JHEP* **08** (2019) 137 [[1907.01556](#)].
- [28] M. Davier, A. Hoecker, B. Malaescu and Z. Zhang, *A new evaluation of the hadronic vacuum polarisation contributions to the muon anomalous magnetic moment and to $\alpha(m_Z^2)$* , *Eur. Phys. J. C* **80** (2020) 241 [[1908.00921](#)].
- [29] A. Keshavarzi, D. Nomura and T. Teubner, *$g - 2$ of charged leptons, $\alpha(M_Z^2)$, and the hyperfine splitting of muonium*, *Phys. Rev. D* **101** (2020) 014029 [[1911.00367](#)].
- [30] M. Davier, A. Hoecker, G. Lopez Castro, B. Malaescu, X.H. Mo, G. Toledo Sanchez et al., *The Discrepancy Between τ and e^+e^- Spectral Functions Revisited and the Consequences for the Muon Magnetic Anomaly*, *Eur. Phys. J. C* **66** (2010) 127 [[0906.5443](#)].
- [31] M. Cè et al., *Window observable for the hadronic vacuum polarization contribution to the muon $g - 2$ from lattice QCD*, [2206.06582](#).

- [32] C. Alexandrou et al., *Lattice calculation of the short and intermediate time-distance hadronic vacuum polarization contributions to the muon magnetic moment using twisted-mass fermions*, [2206.15084](#).
- [33] T. Blum et al., *An update of Euclidean windows of the hadronic vacuum polarization*, [2301.08696](#).
- [34] A. Bazavov et al., *Light-quark connected intermediate-window contributions to the muon $g - 2$ hadronic vacuum polarization from lattice QCD*, [2301.08274](#).
- [35] PARTICLE DATA GROUP collaboration, *Review of Particle Physics*, *PTEP* **2022** (2022) 083C01.
- [36] A. Pich, *Precision physics with inclusive QCD processes*, *Prog. Part. Nucl. Phys.* **117** (2021) 103846 [[2012.04716](#)].
- [37] A. Pich, *Effective field theory: Course*, in *Les Houches Summer School in Theoretical Physics, Session 68: Probing the Standard Model of Particle Interactions*, pp. 949–1049, 6, 1998 [[hep-ph/9806303](#)].
- [38] S. Eidelman, F. Jegerlehner, A.L. Kataev and O. Veretin, *Testing nonperturbative strong interaction effects via the Adler function*, *Phys. Lett. B* **454** (1999) 369 [[hep-ph/9812521](#)].
- [39] F. Jegerlehner, $\alpha_{QED,eff}(s)$ for precision physics at the FCC-ee/ILC, *CERN Yellow Reports: Monographs* **3** (2020) 9.
- [40] F. Le Diberder and A. Pich, *The perturbative QCD prediction to $R(\tau)$ revisited*, *Phys. Lett. B* **286** (1992) 147.
- [41] FLAVOUR LATTICE AVERAGING GROUP (FLAG) collaboration, *FLAG Review 2021*, *Eur. Phys. J. C* **82** (2022) 869 [[2111.09849](#)].
- [42] C. McNeile, C.T.H. Davies, E. Follana, K. Hornbostel and G.P. Lepage, *High-Precision c and b Masses, and QCD Coupling from Current-Current Correlators in Lattice and Continuum QCD*, *Phys. Rev. D* **82** (2010) 034512 [[1004.4285](#)].
- [43] Y.-B. Yang et al., *Charm and strange quark masses and f_{D_s} from overlap fermions*, *Phys. Rev. D* **92** (2015) 034517 [[1410.3343](#)].
- [44] K. Nakayama, B. Fahy and S. Hashimoto, *Short-distance charmonium correlator on the lattice with Möbius domain-wall fermion and a determination of charm quark mass*, *Phys. Rev. D* **94** (2016) 054507 [[1606.01002](#)].
- [45] P. Petreczky and J.H. Weber, *Strong coupling constant and heavy quark masses in $(2+1)$ -flavor QCD*, *Phys. Rev. D* **100** (2019) 034519 [[1901.06424](#)].
- [46] EUROPEAN TWISTED MASS collaboration, *Up, down, strange and charm quark masses with $N_f = 2+1+1$ twisted mass lattice QCD*, *Nucl. Phys. B* **887** (2014) 19 [[1403.4504](#)].
- [47] B. Chakraborty, C.T.H. Davies, B. Galloway, P. Knecht, J. Koponen, G.C. Donald et al., *High-precision quark masses and QCD coupling from $n_f = 4$ lattice QCD*, *Phys. Rev. D* **91** (2015) 054508 [[1408.4169](#)].
- [48] C. Alexandrou, V. Drach, K. Jansen, C. Kallidonis and G. Koutsou, *Baryon spectrum with $N_f = 2 + 1 + 1$ twisted mass fermions*, *Phys. Rev. D* **90** (2014) 074501 [[1406.4310](#)].
- [49] FERMILAB LATTICE, MILC, TUMQCD collaboration, *Up-, down-, strange-, charm-, and bottom-quark masses from four-flavor lattice QCD*, *Phys. Rev. D* **98** (2018) 054517 [[1802.04248](#)].

- [50] HPQCD collaboration, *Charmonium properties from lattice QCD+QED : Hyperfine splitting, J/ψ leptonic width, charm quark mass, and a_μ^c* , *Phys. Rev. D* **102** (2020) 054511 [[2005.01845](#)].
- [51] D. Hatton, C.T.H. Davies, J. Koponen, G.P. Lepage and A.T. Lytle, *Determination of \bar{m}_b/\bar{m}_c and \bar{m}_b from $n_f = 4$ lattice QCD+QED*, *Phys. Rev. D* **103** (2021) 114508 [[2102.09609](#)].
- [52] B. Colquhoun, R.J. Dowdall, C.T.H. Davies, K. Hornbostel and G.P. Lepage, *Υ and Υ' Leptonic Widths, a_μ^b and m_b from full lattice QCD*, *Phys. Rev. D* **91** (2015) 074514 [[1408.5768](#)].
- [53] ETM collaboration, *Mass of the b quark and B -meson decay constants from $N_f=2+1+1$ twisted-mass lattice QCD*, *Phys. Rev. D* **93** (2016) 114505 [[1603.04306](#)].
- [54] P. Gambino, A. Melis and S. Simula, *Extraction of heavy-quark-expansion parameters from unquenched lattice data on pseudoscalar and vector heavy-light meson masses*, *Phys. Rev. D* **96** (2017) 014511 [[1704.06105](#)].
- [55] F. Herren and M. Steinhauser, *Version 3 of RunDec and CRunDec*, *Comput. Phys. Commun.* **224** (2018) 333 [[1703.03751](#)].
- [56] P.A. Baikov, K.G. Chetyrkin and J.H. Kuhn, *Order $\alpha_s^4(s)$ QCD Corrections to Z and τ Decays*, *Phys. Rev. Lett.* **101** (2008) 012002 [[0801.1821](#)].
- [57] M. Beneke and M. Jamin, *α_s and the τ hadronic width: fixed-order, contour-improved and higher-order perturbation theory*, *JHEP* **09** (2008) 044 [[0806.3156](#)].
- [58] D. Boito, P. Masjuan and F. Olyani, *Higher-order QCD corrections to hadronic τ decays from Padé approximants*, *JHEP* **08** (2018) 075 [[1807.01567](#)].
- [59] I. Caprini, *Higher-order perturbative coefficients in QCD from series acceleration by conformal mappings*, *Phys. Rev. D* **100** (2019) 056019 [[1908.06632](#)].
- [60] M. Jamin, *Higher-order behaviour of two-point current correlators*, *Eur. Phys. J. ST* **230** (2021) 2609 [[2106.01614](#)].
- [61] I.O. Goriachuk, A.L. Kataev and V.S. Molokoedov, *The $\overline{\text{MS}}$ -scheme α_s^5 QCD contributions to the Adler function and Bjorken polarized sum rule in the Crewther-type two-fold β -expanded representation*, *JHEP* **05** (2022) 028 [[2111.12060](#)].
- [62] C. Ayala, G. Cvetič and D. Teca, *Borel-Laplace Sum Rules with τ decay data, using OPE with improved anomalous dimensions*, [2206.05631](#).
- [63] A. Pich and A. Rodríguez-Sánchez, *Determination of the QCD coupling from ALEPH τ decay data*, *Phys. Rev. D* **94** (2016) 034027 [[1605.06830](#)].
- [64] G.P. Salam, *The strong coupling: a theoretical perspective*, in *From My Vast Repertoire ...: Guido Altarelli's Legacy*, A. Levy, S. Forte and G. Ridolfi, eds., pp. 101–121 (2019), DOI [[1712.05165](#)].
- [65] L. Del Debbio and A. Ramos, *Lattice determinations of the strong coupling*, [2101.04762](#).
- [66] MILC collaboration, *MILC results for light pseudoscalars*, *PoS CD09* (2009) 007 [[0910.2966](#)].
- [67] S. Durr, Z. Fodor, C. Hoelbling, S.D. Katz, S. Krieg, T. Kurth et al., *Lattice QCD at the physical point: light quark masses*, *Phys. Lett. B* **701** (2011) 265 [[1011.2403](#)].

- [68] S. Durr, Z. Fodor, C. Hoelbling, S.D. Katz, S. Krieg, T. Kurth et al., *Lattice QCD at the physical point: Simulation and analysis details*, *JHEP* **08** (2011) 148 [[1011.2711](#)].
- [69] RBC, UKQCD collaboration, *Domain wall QCD with physical quark masses*, *Phys. Rev. D* **93** (2016) 074505 [[1411.7017](#)].
- [70] HPQCD collaboration, *Determination of quark masses from $\mathbf{n}_f = 4$ lattice QCD and the RI-SMOM intermediate scheme*, *Phys. Rev. D* **98** (2018) 014513 [[1805.06225](#)].
- [71] A.H. Hoang, M. Jezabek, J.H. Kuhn and T. Teubner, *Radiation of heavy quarks*, *Phys. Lett. B* **338** (1994) 330 [[hep-ph/9407338](#)].
- [72] K.G. Chetyrkin, *Power suppressed heavy quark mass corrections to the tau lepton and Z boson decay rates*, *Phys. Lett. B* **307** (1993) 169.
- [73] S.A. Larin, T. van Ritbergen and J.A.M. Vermaseren, *The Large quark mass expansion of $\Gamma(Z^0 \rightarrow \text{hadrons})$ and $\Gamma(\tau^- \rightarrow \nu_\tau + \text{hadrons})$ in the order α_s^3* , *Nucl. Phys. B* **438** (1995) 278 [[hep-ph/9411260](#)].
- [74] B. Dehnadi, A.H. Hoang, V. Mateu and S.M. Zebarjad, *Charm Mass Determination from QCD Charmonium Sum Rules at Order α_s^3* , *JHEP* **09** (2013) 103 [[1102.2264](#)].
- [75] D. Boito and V. Mateu, *Precise α_s determination from charmonium sum rules*, *Phys. Lett. B* **806** (2020) 135482 [[1912.06237](#)].
- [76] K.G. Chetyrkin, J.H. Kuhn and M. Steinhauser, *Heavy quark vacuum polarization to three loops*, *Phys. Lett. B* **371** (1996) 93 [[hep-ph/9511430](#)].
- [77] K.G. Chetyrkin, J.H. Kuhn and M. Steinhauser, *Three loop polarization function and $O(\alpha_s^2)$ corrections to the production of heavy quarks*, *Nucl. Phys. B* **482** (1996) 213 [[hep-ph/9606230](#)].
- [78] K.G. Chetyrkin, J.H. Kuhn and M. Steinhauser, *Heavy quark current correlators to $O(\alpha_s^2)$* , *Nucl. Phys. B* **505** (1997) 40 [[hep-ph/9705254](#)].
- [79] A. Maier, P. Maierhofer and P. Marquard, *Higher Moments of Heavy Quark Correlators in the Low Energy Limit at $O(\alpha_s^2)$* , *Nucl. Phys. B* **797** (2008) 218 [[0711.2636](#)].
- [80] R. Boughezal, M. Czakon and T. Schutzmeier, *Four-Loop Tadpoles: Applications in QCD*, *Nucl. Phys. B Proc. Suppl.* **160** (2006) 160 [[hep-ph/0607141](#)].
- [81] K.G. Chetyrkin, J.H. Kuhn and C. Sturm, *Four-loop moments of the heavy quark vacuum polarization function in perturbative QCD*, *Eur. Phys. J. C* **48** (2006) 107 [[hep-ph/0604234](#)].
- [82] R. Boughezal, M. Czakon and T. Schutzmeier, *Charm and bottom quark masses from perturbative QCD*, *Phys. Rev. D* **74** (2006) 074006 [[hep-ph/0605023](#)].
- [83] A. Maier, P. Maierhofer and P. Marquard, *The Second physical moment of the heavy quark vector correlator at $O(\alpha_s^3)$* , *Phys. Lett. B* **669** (2008) 88 [[0806.3405](#)].
- [84] A. Maier, P. Maierhofer, P. Marquard and A.V. Smirnov, *Low energy moments of heavy quark current correlators at four loops*, *Nucl. Phys. B* **824** (2010) 1 [[0907.2117](#)].
- [85] A. Maier and P. Marquard, *Validity of Padé approximations in vacuum polarization at three- and four-loop order*, *Phys. Rev. D* **97** (2018) 056016 [[1710.03724](#)].
- [86] A.H. Hoang, V. Mateu and S. Mohammad Zebarjad, *Heavy Quark Vacuum Polarization Function at $O(\alpha_s^2)$ and $O(\alpha_s^3)$* , *Nucl. Phys. B* **813** (2009) 349 [[0807.4173](#)].

- [87] Y. Kiyo, A. Maier, P. Maierhofer and P. Marquard, *Reconstruction of heavy quark current correlators at $O(\alpha_s^3)$* , *Nucl. Phys. B* **823** (2009) 269 [0907.2120].
- [88] S. Groote and A.A. Pivovarov, *Low-energy gluon contributions to the vacuum polarization of heavy quarks*, *JETP Lett.* **75** (2002) 221 [hep-ph/0103047].
- [89] A.L. Kataev, *Higher order $O(\alpha^2)$ and $O(\alpha\alpha_s)$ corrections to $\sigma_{\text{tot}}(e^+e^- \rightarrow \text{hadrons})$ and Z -boson decay rate*, *Phys. Lett. B* **287** (1992) 209.
- [90] C. Ayala, X. Lobregat and A. Pineda, *Determination of $\alpha(M_Z)$ from an hyperasymptotic approximation to the energy of a static quark-antiquark pair*, *JHEP* **09** (2020) 016 [2005.12301].
- [91] TUMQCD collaboration, *Determination of the QCD coupling from the static energy and the free energy*, *Phys. Rev. D* **100** (2019) 114511 [1907.11747].
- [92] S. Cali, K. Cichy, P. Korcyl and J. Simeth, *Running coupling constant from position-space current-current correlation functions in three-flavor lattice QCD*, *Phys. Rev. Lett.* **125** (2020) 242002 [2003.05781].
- [93] ALPHA collaboration, *QCD Coupling from a Nonperturbative Determination of the Three-Flavor Λ Parameter*, *Phys. Rev. Lett.* **119** (2017) 102001 [1706.03821].
- [94] PACS-CS collaboration, *Precise determination of the strong coupling constant in $N_f = 2+1$ lattice QCD with the Schrödinger functional scheme*, *JHEP* **10** (2009) 053 [0906.3906].
- [95] K. Maltman, D. Leinweber, P. Moran and A. Sternbeck, *The Realistic Lattice Determination of $\alpha(s)(M(Z))$ Revisited*, *Phys. Rev. D* **78** (2008) 114504 [0807.2020].
- [96] M. Davier, A. Hoecker, B. Malaescu, C.Z. Yuan and Z. Zhang, *Reevaluation of the hadronic contribution to the muon magnetic anomaly using new $e^+e^- \rightarrow \pi^+\pi^-$ cross section data from BABAR*, *Eur. Phys. J. C* **66** (2010) 1 [0908.4300].
- [97] M. Davier, A. Hoecker, B. Malaescu and Z. Zhang, *Reevaluation of the Hadronic Contributions to the Muon $g - 2$ and to $\alpha(M_Z)$* , *Eur. Phys. J. C* **71** (2011) 1515 [1010.4180].
- [98] BABAR collaboration, *Precise measurement of the $e^+e^- \rightarrow \pi^+\pi^-(\gamma)$ cross section with the Initial State Radiation method at BABAR*, *Phys. Rev. Lett.* **103** (2009) 231801 [0908.3589].
- [99] BABAR collaboration, *Precise Measurement of the $e^+e^- \rightarrow \pi^+\pi^-(\gamma)$ Cross Section with the Initial-State Radiation Method at BABAR*, *Phys. Rev. D* **86** (2012) 032013 [1205.2228].
- [100] KLOE collaboration, *Measurement of $\sigma(e^+e^- \rightarrow \pi^+\pi^-\gamma(\gamma))$ and the dipion contribution to the muon anomaly with the KLOE detector*, *Phys. Lett. B* **670** (2009) 285 [0809.3950].
- [101] KLOE collaboration, *Measurement of $\sigma(e^+e^- \rightarrow \pi^+\pi^-)$ from threshold to 0.85 GeV^2 using Initial State Radiation with the KLOE detector*, *Phys. Lett. B* **700** (2011) 102 [1006.5313].
- [102] KLOE collaboration, *Precision measurement of $\sigma(e^+e^- \rightarrow \pi^+\pi^-\gamma)/\sigma(e^+e^- \rightarrow \mu^+\mu^-\gamma)$ and determination of the $\pi^+\pi^-$ contribution to the muon anomaly with the KLOE detector*, *Phys. Lett. B* **720** (2013) 336 [1212.4524].
- [103] CMD-3 collaboration, *Measurement of the $e^+e^- \rightarrow \pi^+\pi^-$ cross section from threshold to 1.2 GeV with the CMD-3 detector*, [2302.08834](#).
- [104] V.M. Aul'chenko et al., *Measurement of the $e^+e^- \rightarrow \pi^+\pi^-$ cross section with the CMD-2 detector in the $370\text{-}520 \text{ MeV}$ c.m. energy range*, *JETP Lett.* **84** (2006) 413 [hep-ex/0610016].

- [105] CMD-2 collaboration, *High-statistics measurement of the pion form factor in the rho-meson energy range with the CMD-2 detector*, *Phys. Lett. B* **648** (2007) 28 [[hep-ex/0610021](#)].
- [106] BESIII collaboration, *Measurement of the Cross Section for $e^+e^- \rightarrow \text{Hadrons}$ at Energies from 2.2324 to 3.6710 GeV*, *Phys. Rev. Lett.* **128** (2022) 062004 [[2112.11728](#)].
- [107] Y. Aoki et al., *FLAG Review 2021*, [2111.09849](#).
- [108] M. Dalla Brida, R. Höllwieser, F. Knechtli, T. Korzec, A. Nada, A. Ramos et al., *Determination of $\alpha_s(m_Z)$ by the non-perturbative decoupling method*, [2209.14204](#).
- [109] A. Pich and A. Rodríguez-Sánchez, *SU(3) analysis of four-quark operators: $K \rightarrow \pi\pi$ and vacuum matrix elements*, *JHEP* **06** (2021) 005 [[2102.09308](#)].
- [110] M. González-Alonso, A. Pich and A. Rodríguez-Sánchez, *Updated determination of chiral couplings and vacuum condensates from hadronic τ decay data*, *Phys. Rev. D* **94** (2016) 014017 [[1602.06112](#)].
- [111] S. Narison, $\bar{m}_{c,b}, < \alpha_s G^2 >$ and α_s from Heavy Quarkonia, *Nucl. Part. Phys. Proc.* **300-302** (2018) 153.
- [112] P. Gubler and D. Satow, *Recent Progress in QCD Condensate Evaluations and Sum Rules*, *Prog. Part. Nucl. Phys.* **106** (2019) 1 [[1812.00385](#)].
- [113] A. Pich, *Chiral perturbation theory*, *Rept. Prog. Phys.* **58** (1995) 563 [[hep-ph/9502366](#)].
- [114] M. Gell-Mann, R.J. Oakes and B. Renner, *Behavior of current divergences under SU(3) x SU(3)*, *Phys. Rev.* **175** (1968) 2195.
- [115] A. Pich and J. Prades, *Strange quark mass determination from Cabibbo suppressed tau decays*, *JHEP* **10** (1999) 004 [[hep-ph/9909244](#)].
- [116] M. Jamin, *Flavor symmetry breaking of the quark condensate and chiral corrections to the Gell-Mann-Oakes-Renner relation*, *Phys. Lett. B* **538** (2002) 71 [[hep-ph/0201174](#)].
- [117] E. Gamiz, M. Jamin, A. Pich, J. Prades and F. Schwab, *Determination of m_s and $|V_{us}|$ from hadronic tau decays*, *JHEP* **01** (2003) 060 [[hep-ph/0212230](#)].
- [118] M. Davier, A. Höcker, B. Malaescu, C.-Z. Yuan and Z. Zhang, *Update of the ALEPH non-strange spectral functions from hadronic τ decays*, *Eur. Phys. J. C* **74** (2014) 2803 [[1312.1501](#)].
- [119] A. Pich and A. Rodríguez-Sánchez, *Violations of quark-hadron duality in low-energy determinations of α_s* , *JHEP* **07** (2022) 145 [[2205.07587](#)].
- [120] V. Cirigliano, D. Díaz-Calderón, A. Falkowski, M. González-Alonso and A. Rodríguez-Sánchez, *Semileptonic tau decays beyond the Standard Model*, *JHEP* **04** (2022) 152 [[2112.02087](#)].
- [121] L. Lyons, A.J. Martin and D.H. Saxon, *On the Determination of the B Lifetime by Combining the Results of Different Experiments*, *Phys. Rev. D* **41** (1990) 982.
- [122] G. D'Agostini, *On the use of the covariance matrix to fit correlated data*, *Nucl. Instrum. Meth. A* **346** (1994) 306.
- [123] V. Blobel, *Some Comments on χ^2 Minimization Applications*, *eConf* **C030908** (2003) MOET002.
- [124] C. Pascaud and F. Zomer, *QCD analysis from the proton structure function F_2 measurement: Issues on fitting, statistical and systematic errors*, *LAL-95-05* (1995) .

- [125] ATLAS collaboration, *Jet energy measurement and its systematic uncertainty in proton-proton collisions at $\sqrt{s} = 7$ TeV with the ATLAS detector*, *Eur. Phys. J. C* **75** (2015) 17 [1406.0076].
- [126] ATLAS collaboration, *Measurement of the inclusive jet cross-sections in proton-proton collisions at $\sqrt{s} = 8$ TeV with the ATLAS detector*, *JHEP* **09** (2017) 020 [1706.03192].
- [127] ATLAS collaboration, *Measurement of inclusive jet and dijet cross-sections in proton-proton collisions at $\sqrt{s} = 13$ TeV with the ATLAS detector*, *JHEP* **05** (2018) 195 [1711.02692].
- [128] B. Malaescu, “Treatment of uncertainties and correlations in combinations of e^+e^- annihilation data.” <https://indico.him.uni-mainz.de/event/11/session/1/contribution/42/material/slides/0.pdf>, 2018.
- [129] T. Aoyama et al., *The anomalous magnetic moment of the muon in the Standard Model*, *Phys. Rept.* **887** (2020) 1 [2006.04822].
- [130] G. Cowan, *Effect of Systematic Uncertainty Estimation on the Muon $g - 2$ Anomaly*, *EPJ Web Conf.* **258** (2022) 09002 [2107.02652].
- [131] G. Cowan, *Statistical data analysis* (1998).
- [132] PARTICLE DATA GROUP collaboration, *Review of particle physics*, *J. Phys. G* **37** (2010) 075021.
- [133] B. Malaescu and P. Starovoitov, *Evaluation of the Strong Coupling Constant α_s Using the ATLAS Inclusive Jet Cross-Section Data*, *Eur. Phys. J. C* **72** (2012) 2041 [1203.5416].
- [134] R. Nisius, *On the combination of correlated estimates of a physics observable*, *Eur. Phys. J. C* **74** (2014) 3004 [1402.4016].
- [135] O.V. Tarasov, A.A. Vladimirov and A.Y. Zharkov, *The Gell-Mann-Low Function of QCD in the Three Loop Approximation*, *Phys. Lett. B* **93** (1980) 429.
- [136] T. van Ritbergen, J.A.M. Vermaseren and S.A. Larin, *The Four loop beta function in quantum chromodynamics*, *Phys. Lett. B* **400** (1997) 379 [hep-ph/9701390].
- [137] M. Czakon, *The Four-loop QCD beta-function and anomalous dimensions*, *Nucl. Phys. B* **710** (2005) 485 [hep-ph/0411261].
- [138] P.A. Baikov, K.G. Chetyrkin and J.H. Kühn, *Five-Loop Running of the QCD coupling constant*, *Phys. Rev. Lett.* **118** (2017) 082002 [1606.08659].
- [139] T. Luthe, A. Maier, P. Marquard and Y. Schröder, *Towards the five-loop Beta function for a general gauge group*, *JHEP* **07** (2016) 127 [1606.08662].
- [140] F. Herzog, B. Ruijl, T. Ueda, J.A.M. Vermaseren and A. Vogt, *The five-loop beta function of Yang-Mills theory with fermions*, *JHEP* **02** (2017) 090 [1701.01404].
- [141] T. Luthe, A. Maier, P. Marquard and Y. Schroder, *Complete renormalization of QCD at five loops*, *JHEP* **03** (2017) 020 [1701.07068].
- [142] T. Luthe, A. Maier, P. Marquard and Y. Schroder, *The five-loop Beta function for a general gauge group and anomalous dimensions beyond Feynman gauge*, *JHEP* **10** (2017) 166 [1709.07718].
- [143] K.G. Chetyrkin, G. Falcioni, F. Herzog and J.A.M. Vermaseren, *Five-loop renormalisation of QCD in covariant gauges*, *JHEP* **10** (2017) 179 [1709.08541].

- [144] O.V. Tarasov, *Anomalous dimensions of quark masses in the three-loop approximation*, *Phys. Part. Nucl. Lett.* **17** (2020) 109 [[1910.12231](#)].
- [145] S.A. Larin, *The Renormalization of the axial anomaly in dimensional regularization*, *Phys. Lett. B* **303** (1993) 113 [[hep-ph/9302240](#)].
- [146] K.G. Chetyrkin, *Quark mass anomalous dimension to $O(\alpha_s^4)$* , *Phys. Lett. B* **404** (1997) 161 [[hep-ph/9703278](#)].
- [147] J.A.M. Vermaseren, S.A. Larin and T. van Ritbergen, *The four loop quark mass anomalous dimension and the invariant quark mass*, *Phys. Lett. B* **405** (1997) 327 [[hep-ph/9703284](#)].
- [148] P.A. Baikov, K.G. Chetyrkin and J.H. Kühn, *Quark Mass and Field Anomalous Dimensions to $O(\alpha_s^5)$* , *JHEP* **10** (2014) 076 [[1402.6611](#)].
- [149] T. Luthe, A. Maier, P. Marquard and Y. Schröder, *Five-loop quark mass and field anomalous dimensions for a general gauge group*, *JHEP* **01** (2017) 081 [[1612.05512](#)].
- [150] P.A. Baikov, K.G. Chetyrkin and J.H. Kühn, *Five-loop fermion anomalous dimension for a general gauge group from four-loop massless propagators*, *JHEP* **04** (2017) 119 [[1702.01458](#)].
- [151] T. Appelquist and H. Georgi, *$e^+ e^-$ annihilation in gauge theories of strong interactions*, *Phys. Rev. D* **8** (1973) 4000.
- [152] A. Zee, *Electron positron annihilation in stagnant field theories*, *Phys. Rev. D* **8** (1973) 4038.
- [153] K.G. Chetyrkin, A.L. Kataev and F.V. Tkachov, *Higher Order Corrections to Sigma-t ($e^+ e^- \rightarrow$ Hadrons) in Quantum Chromodynamics*, *Phys. Lett. B* **85** (1979) 277.
- [154] M. Dine and J.R. Sapirstein, *Higher Order QCD Corrections in $e^+ e^-$ Annihilation*, *Phys. Rev. Lett.* **43** (1979) 668.
- [155] S.G. Gorishnii, A.L. Kataev and S.A. Larin, *The $O(\alpha_s^3)$ -corrections to $\sigma_{tot}(e^+e^- \rightarrow$ hadrons) and $\Gamma(\tau^- \rightarrow \nu_\tau +$ hadrons) in QCD*, *Phys. Lett. B* **259** (1991) 144.
- [156] L.R. Surguladze and M.A. Samuel, *Total hadronic cross-section in e^+e^- annihilation at the four loop level of perturbative QCD*, *Phys. Rev. Lett.* **66** (1991) 560.
- [157] K.G. Chetyrkin, *Corrections of order α_s^3 to R_{had} in pQCD with light gluinos*, *Phys. Lett. B* **391** (1997) 402 [[hep-ph/9608480](#)].
- [158] P.A. Baikov, K.G. Chetyrkin and J.H. Kuhn, *Adler Function, Bjorken Sum Rule, and the Crewther Relation to Order α_s^4 in a General Gauge Theory*, *Phys. Rev. Lett.* **104** (2010) 132004 [[1001.3606](#)].
- [159] F. Herzog, B. Ruijl, T. Ueda, J.A.M. Vermaseren and A. Vogt, *On Higgs decays to hadrons and the R-ratio at N^4LO* , *JHEP* **08** (2017) 113 [[1707.01044](#)].
- [160] S.C. Generalis, *Improved two loop quark mass corrections*, *J. Phys. G* **15** (1989) L225.
- [161] K.G. Chetyrkin and A. Kwiatkowski, *Mass corrections to the tau decay rate*, *Z. Phys. C* **59** (1993) 525 [[hep-ph/9805232](#)].
- [162] S.G. Gorishnii, A.L. Kataev and S.A. Larin, *Three Loop Corrections of Order $O(m^2)$ to the Correlator of Electromagnetic Quark Currents*, *Nuovo Cim. A* **92** (1986) 119.
- [163] W. Bernreuther and W. Wetzel, *Order α_s^2 Massive Quark Contribution to the Vacuum Polarization of Massless Quarks*, *Z. Phys. C* **11** (1981) 113.

- [164] P.A. Baikov, K.G. Chetyrkin and J.H. Kuhn, *Vacuum polarization in pQCD: First complete $O(\alpha_s^4)$ result*, *Nucl. Phys. B Proc. Suppl.* **135** (2004) 243.